Effects of thermophysical, hydrodynamics and thermal characteristics of well stable metallic nanofluids on energy transportation

Waqar Ahmed[1,2] · Nor Azwadi Che Sidik[1] · Shahid Mehmood[3] · Mir Waqas Alam[4] · H. Fayaz[5] ·
Muhammad Iqbal Hussain[6] · Omer A. Alawi[7] · Syed Muzamil Ahmed[8] · Syed Nadeem Abbas Shah[9] · S. N. Kazi[10]

Abstract

The current research focuses on the chemical synthesis of ZnO and preparation of ZnO dispersed in EG@DW mixture-based nanofluids for the investigation of enhancement in heat transfer of a square shaped heat exchanger. The steady and uniform dispersion of ZnO nanoparticles was achieved using high probe sonication at varying mass% concentrations like (0.1; 0.075; 0.05 and 0.025 mass%). Also, the ZnO particles were synthesized using sonochemical technique, where sodium hydroxide (NaOH) and zinc acetate ($ZnC_4H_6O_4$) were used as raw materials. For the verification of ZnO synthesis numerous characterizations like UV–Vis, XRD, FTIR, and FESEM analysis were carried out. The changed mass% concentrations of ZnO-EG@DW-based nanofluids were considered to check their effects on thermophysical properties, dispersion, stability, and heat transfer (Nusselt Numbers) at varying Reynolds numbers ranging from 4550 to 20,360 using square heat exchanger. A positive increase in thermal conductivity was observed by the addition of ZnO in the ZnO-EG@DW with (50:50) mixture. The highest thermal conductivity of 1.0 W m^{-1} K^{-1} was noticed at a maximum of 0.1 mass% concentration which is greater than base fluid (EG@DW) at 45 °C. The maximum pressure drop of 2400 Pa m^{-1} at Reynold number 20360 and higher friction loss of 0.045 for Reynolds number 4550 was noticed at 0.1 mass% concentration. The highest improvement in heat transfer was recorded at 0.1 mass% is 550–2830 W m^{-1} K which is 63% greater of the base fluid, while others mass% illustrate improved heat transfer coefficient of about 550–2170, 550–1750, and 550–1500 W m^{-2} K^{-1}, respectively, at highest Reynolds (Re) when it compared with the base fluid (EG@DW). All the heat transfer related experiments were executed at 30 °C room temperature where constant heat flux of 10,886 W m^{-2} and eight varying flow rates were used.

✉ Waqar Ahmed
ahmed.waqar@utm.my; waqarum.ah@gmail.com

✉ Nor Azwadi Che Sidik
azwadi@utm.my

✉ S. N. Kazi
salimnewaz@um.edu.my

1 Takasago I-Kohza, Malaysia-Japan International Institute of Technology, Universiti Teknologi Malaysia, 54100 Kuala Lumpur, Malaysia

2 Institute for Advanced Studies, University of Malaya, 50603 Kuala Lumpur, Malaysia

3 School of Integrated Science and Innovation (ISI), Sirindhorn International Institute of Technology (SIIT), Thammasat University, Pathum Thani 12121, Thailand

4 Department of Physics, College of Science, King Faisal University, Al Ahsa 31982, Saudi Arabia

5 Modeling Evolutionary Algorithms Simulation and Artificial Intelligence, Faculty of Electrical & Electronics Engineering, Ton Duc Thang University, Ho Chi Minh City, Viet Nam

6 Faculty of Mechanical Engineering Technology (FTKM), Universiti Malaysia Perlis (UniMap) Kampus Alam UniMAP, Pauh Putra, 02600 Arau, Perlis, Malaysia

7 Department of Thermofluids, School of Mechanical Engineering, Universiti Teknologi Malaysia, 81310 UTM Skudai, Johor Bahru, Malaysia

8 Faculty of Engineering, University of Malaya, 50603 Kuala Lumpur, Malaysia

9 Department of Mechanical Engineering (Main Campus Lahore), University of Engineering and Technology Lahore, 54890 Lahore, Pakistan

10 Department of Mechanical Engineering, Faculty of Engineering, University of Malaya, 50603 Kuala Lumpur, Malaysia

Graphical abstract
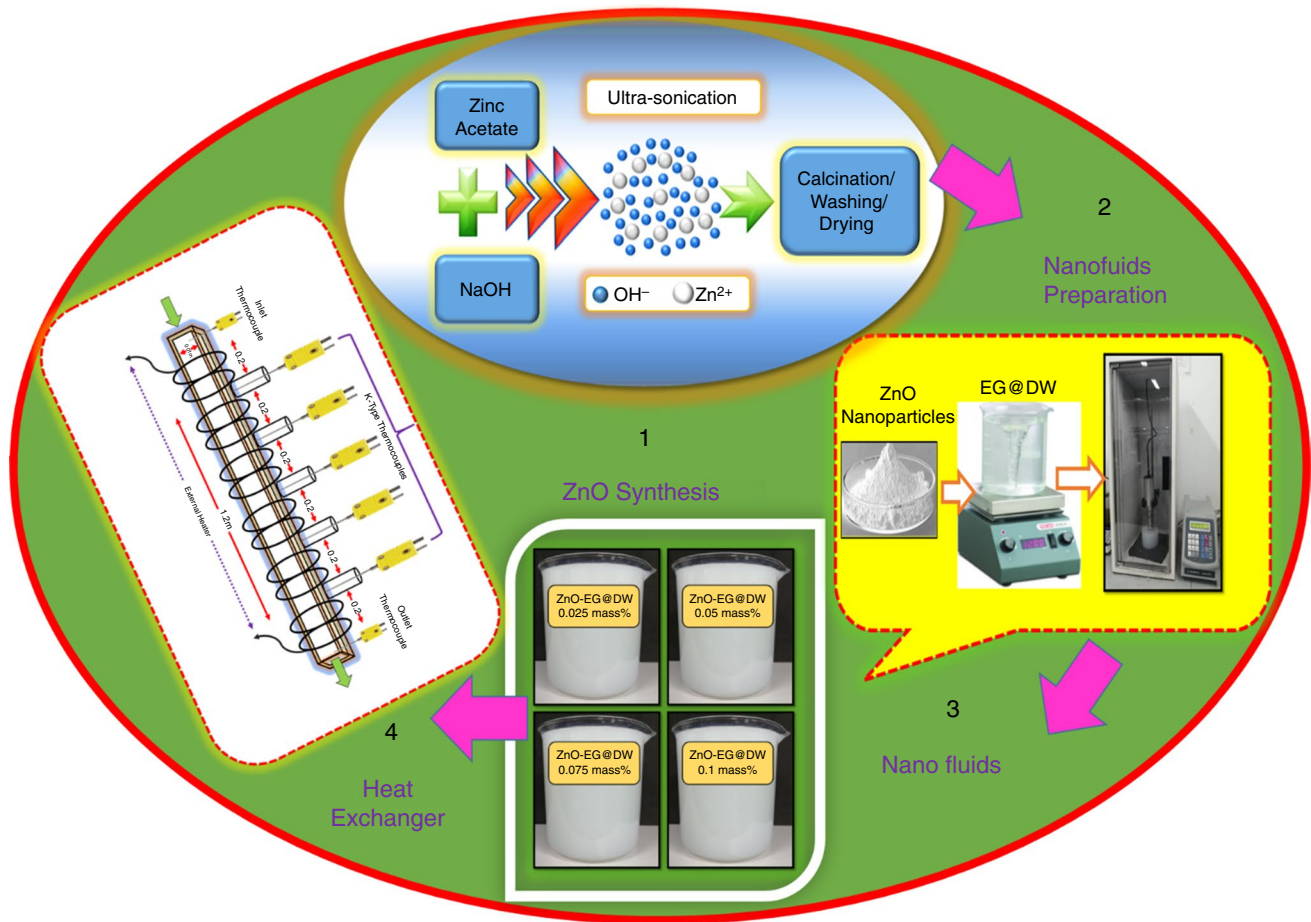
Keywords ZnO synthesis · Nanofluids preparation · Thermal conductivity · Viscosity · Heat transfer coefficient

List of symbols

EG	Ethylene glycol
N_P	Nanoparticles
N_f	Nanofluids
DW	Distilled water
C_f	Friction coefficient
Cu	Copper
C_p	Specific heat
d_p	Nanoparticles diameter
Conc	Concentration
K	Thermal conductivity
R	Ratio of materials
T	Temperature
h	Convective heat transfer coefficient
Nu	Nusselt numbers
Q	Heat flux
L	Length of medium

Greek symbols and subscript

W	Wall
F	Fluid
B_f	Base fluid
T	Turbulence
FF	Friction factor
P	Density in kg m^{-3}
μ	Dynamic viscosity in N m s^{-1}
Φ	% Volume friction
V	Kinematic viscosity m^2 s^{-2}
ϕ	Volume friction

Introduction

The ever increasing demand for efficient heat transportation solutions has come to be a key challenge for engineering and manufacturing productions especially in power and energy

sectors. The aim of this research is based on the application of different mediums in the heat transfer process. Usually, normal or distilled water was used previously as a heat carrier specifically in oil and gas refineries, coal power plants, nuclear plants, and heating and cooling systems, etc. [1]. However, it is observed that the conventional fluids show few drawbacks, specifically on their aspect of heat transfer capability. The results arise from conventional fluids subjected to integrally less thermal conductivity which can be a major cause of attaining low heat exchanges [2, 3]. Therefore, this loss has encouraged several researchers to determine alternative approaches for the improvement of heat transfer in different heat exchangers with their shapes, sizes, surfaces, etc., with improved heat transport characteristics [4–6].

The heat exchangers with varying geometries are being used in engineering industries for heat transfer, which are commonly known as energy-efficient vehicles with less maintenance cost and can be used for a long duration [7]. These heat exchangers are mostly designed according to the apparatus characteristics comprising the fluid, base fluid temperature, heat flux, flow rates, and their dimension as well [8]. Due to their particular shape and design, heat exchangers can be classified into different categories such as heat exchangers with wick, thermosyphon heat exchangers, looped heat exchangers, and looped thermosyphon. Each category of the heat exchanger is suitable for specific applications due to their performance, heat transfer rate, and an impartial system for cooling and due to their installation reasons [9–11].

The more quality of nanofluids as heat transportation fluids could attain by adding the highly conductive nanoparticles (solids) in varying conventional fluids. Choi et al. [12] was the first researcher who coined the term nanofluids, he realized that homogeneous and uniform dispersion of solid nanoparticles in conventional base fluids likewise water, distilled water, Polyethylene glycol (PEG), Palm oil (PO), EG, Diathermic oil (DTO), Transformer oil (TO), glycerin, etc., may illustrate the remarkable improvement in their thermal performances characteristics [13, 14]. The metal oxides, ceramics, carbon structure, and various bio-based particles were used earlier to prepare varying nanofluids. These nanofluids were included Al_2O_3, ZnO, TiO_2, SiO_2, Al/Al_2O_3, Cu/Cupric, CNTs, SWCNTs, and MWCNTs, etc. [15, 16]. Several investigations were conducted on heat transfer improvement by mixing different nanoparticles in normal or distilled water. The importance of distilled water and ethylene glycol as Nano-coolants with the addition of ZnO nanoparticles [17]. The addition of sonochemically synthesized ZnO nanoparticles in EG + DW base fluid with a stable dispersion and longer suspension stability will be a new approach to see heat transfer development of the square heat exchanger [18–20].

Hosseini et al. [21] used Graphene oxide and Al_2O_3 water-based nanofluids at 0.2 mass% concentration of each in the parabolic trough solar collector (PTSC) for the improvement of thermal efficiency. Varied thermo-physical characteristics like dynamic/kinematic viscosities, densities, specific heat and thermal conductivities were also analyzed here. The maximum 23.4% in dynamic viscosity and 9.1% enhancement in thermal conductivity were reported here. Furthermore, three different 1, 3, and 5 L/mint Graphene-based and Al_2O_3-based nanofluids were tested for thermal efficiency, where 63.2% for Graphene oxide and 32.1% for Al_2O_3 enhancement at 1 mass% have been reported.

Said, Z et al. [22] investigated the TiO_2- and Al_2O_3-based nanofluids for thermal enhancement of the radiator. The solid TiO_2 and Al_2O_3 nanoparticles were dispersed in water and EG at a 50:50 ratio each, respectively. Further, different characterizations and thermo-physical properties were analyzed to measure the thermal performance at a 0.3% volume fraction of each. The choice of these metal oxide-based nanofluids was chosen due to their anti-corrosive properties. The highest improvement in heat transfer was observed about 24.21% for Al_2O_3-based nanofluids, which is more than water-, EG-, and TiO_2-based nanofluids.

Saedodin, S et al. [23] has used varying metal oxide-based and turbulator Nano-fluids for heat transfer improvement in a straight tube based on empirical correlation data. The SiO2-/water-based nanofluids were prepared at varying 0.5–2% volume concentrations, where all the volume concentrations have been investigated for the pressure drop and heat transfer improvement. The thermophysical characteristics like dynamic/kinematic viscosity and thermal conductivity were investigated as well. Therefore, based on all these properties the maximum 7.93% heat transfer improvement and 13.96% surge of pressure drop were recorded at a maximum 2% volume concentration. Also, overall 4.2% thermal performance was reported here. Further, this enhancement was compared with metal oxide type nanofluids like TiO_2, Al_2O_3, CuO, and SiO_2 at the same highest 2% volume concentration. In conclusion, the CuO-/water-based nanofluids had better thermal performance as compared to all other nanofluids.

Mahani, R.B et al. [24] studied the heat transfer improvement by combining factor effects, including 3D modeling with varying geometries, and using hybrid nanofluids of Al_2O_3 and Cu at high Reynolds value. The outcomes describe that hybrid nanofluids, Reynolds numbers, and turbulators were influenced to augment the heat transfer enhancement of the rectangular turbulators. By changing the size of turbulators, nanofluids volume fraction, and Reynolds numbers from lower to higher would cause to increase in heat transfer up to 49.17% of the total. The suggested

factors are more practical and can be benefited in the field of nanofluids and fluid mechanisms.

Nafchi, P.M., et al. used ethylene glycol (EG) as a base fluid or dispersant as an antifreeze agent in various engineering-based applications like cooling systems, heat exchangers, automobile radiators, solar collectors, refrigeration, etc. Varying thermophysical and thermal properties were analyzed and outcomes are reported accordingly. However, it has been noticed that this base liquid showed less thermal conductivity as a working fluid in thermal engineering systems [25, 26]. Furthermore, similarly, numerous studies were executed to improve its thermal conductivity and other thermophysical properties such as viscosity, density, and specific heat that can play a vital role in enhanced heat transportation. For this purpose different solid nanoparticles have been used to prepare the ethylene glycol (EG)-based nanofluids at varying mass% concentrations [27, 28].

Also, several researchers have investigated the effects of metal oxide nanoparticles in ethylene glycol (EG) or its mixture on the heat transfer, the results showed improved heat transfer amount with an escalation in concentrations of solid nanoparticles. The addition of highly conductive Nano-sized solid particles in ethylene glycol (EG) or its mixture with water gives an escalation in the thermal conductivity, which may lead to augmented heat transfer [29, 30]. Further, many researchers have revealed the benefits of using different nanofluids in engineering applications such as boiling heat transfer, machining, convective heat transfer, micro-heat exchangers, and cooling [31].

The ultra-sonochemical is a very common technique that has been used for Nano-size particle synthesis in bulk and their varying nanofluids for different purposes. This technique is very useful to produce primarily nanoparticles of regular shape and size, and it is a less time-consuming method as compared to other techniques. Further, solid metal oxide nanoparticles need high sonication to disperse them uniformly and homogeneously in the base fluid. So, for this purpose, the high probe sonication or ultra-sonochemical technique is the best choice, based on these parameters they would prefer this technique throughout the experiment.

Research significance

The previous studies showed a lack of longer dispersion and stability of nanofluids, and they used varying stabilizing agents/surfactants that could drop their thermal conductivities. Still, none of the studies has reported varying improved thermophysical and heat transfer properties of the nanofluids together. Also, pure ethylene glycol-based nanofluids showed higher viscosity which needs additional pumping power which may drop down the efficiency of the system. Similarly, the only distilled water-based nanofluids have dispersion and stability problems. The current study was conducted considering the following key objectives.

- The key objectives of this study are to synthesize ZnO by sonochemical procedure and then using a two-step method for the preparation of surfactant-free stable and homogeneously dispersed ZnO-EG@DW-based nanofluids at different mass% concentrations of (0.1; 0.075; 0.05 and 0.025 mass%) EG@DW (50:50)-based fluid.
- The current study intends to achieve supreme heat transfer "h" in a square shaped heat exchanger. Moreover, the mixture of EG@DW with (50:50) ratio was used as a base fluid for nanofluids preparation.
- A high probe sonication procedure was implemented to enhance and prolong the dispersion/suspension and maximum stability of ZnO in the mixture of EG@DW base fluid. This distinct procedure increases the solid particle dispersion in EG@DW without using any surfactant/stabilizing agent, which can lift their stability.
- In the current study, changing flow rate and uniform heat flux conditions and their effects on the increase in heat transfer (Nusselt numbers) at several localities of square heat exchanger in the turbulent regimes were considered for the EG@DW and ZnO-EG@DW nanofluids at (0.1; 0.075; 0.05 and 0.025 mass%) concentrations.

Methodology and materials

Materials

The zinc acetate dihydrate $Zn(CH_3CO_2)_2 \cdot 2H_2O$ with (99.5%) purity were used as a precursor for ZnO synthesis, sodium hydroxide (NaOH) analytical reagent with (99.%) purity was used as a strong base for chemical reaction with precursor salt, Ethylene glycol (EG) and distilled water (DW) were procured from Sigma Aldrich, Sdn Bhd Selangor Malaysia. Ethylene glycol (EG) with molecular weight (M Wt 62,07) g mol and distilled water were used to synthesis the ZnO nanoparticles by using a one-pot sonochemical procedure. All these chemicals used for synthesis were of analytical grades. Furthermore, a 2-step probe sonication process was adopted to prepare the well dispersed ZnO-EG@DW-based nanofluids at varying (0.1, 0.075, 0.05, and 0.025 mass%) concentrations.

Synthesis of ZnO nanoparticles

The one-pot sonochemical synthesis procedure was used to synthesize the ZnO nanoparticles. Our synthesis process is

quite simple and aims at realizing the efficiency of sono-chemical waves produced by sonicator and the use of precursors and bases in controlling the size. For ZnO synthesis, 1 M zinc acetate Zn $(CH_3COO)_2H_2O$ precursor were added in a mixture of EG@DW with 50:50 and stirred until completely dissolved. A 2 M sodium hydroxide (NaOH) base was added in EG@DW mixture with 50:50 ratios under continuously stirring to prepare the reaction solution. Further, the precursor solution has been kept under probe sonication and the sodium hydroxide NaOH solution was added drop by drop (1 drop/s) into zinc acetate solution under continuous probe sonication for 2 h shown in Fig. 1. The probe amplitude was attuned at 70 with 3/2 s off/on time. The maximum 750 W probe power, 36,000 J delivered energy by the probe, 220 input voltage was selected and the probe temperature was kept at 0 °C. By mixing the NaOH solution into the zinc acetate Zn $(CH_3COO)_2$ H_2O solution, the chemical reaction has started and white precipitate started to form in the EG@DW mixture. After adding the NaOH solution to the zinc acetate solution, both solutions were left for continuous sonication for 3 h. After completing 3 h, these white precipitates were completely transformed into dense white precipitates. After sonication, the dense white precipitates were washed repeatedly with DW and ethanol and finally dried in a vacuum oven for 2 h at 70 °C. Finally, the dried white powder was kept for calcination in a furnace at 200 °C, and ZnO nanoparticles were achieved with spherical morphology, which later on was characterized and confirmed. The chemical reduction process for ZnO nanoparticles is as follows [32].
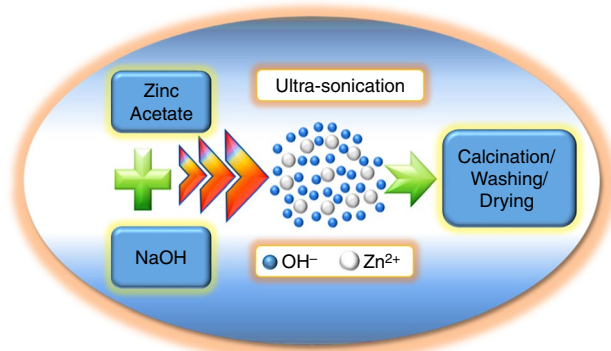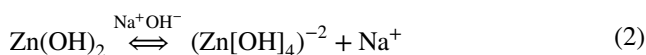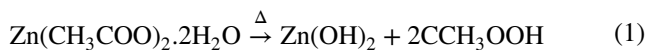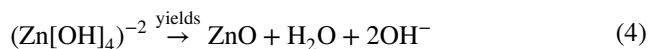
$$Zn(CH_3COO)_2.2H_2O \xrightarrow{\Delta} Zn(OH)_2 + 2CCH_3OOH \qquad (1)$$

$$Zn(OH)_2 \overset{Na^+OH^-}{\Longleftrightarrow} (Zn[OH]_4)^{-2} + Na^+ \qquad (2)$$

$$(Zn[OH]_4)^{-2} \overset{H^+OH^-}{\Longleftrightarrow} (Zn[OH]_4)^{-2} + H^+ \qquad (3)$$

$$(Zn[OH]_4)^{-2} \xrightarrow{yields} ZnO + H_2O + 2OH^- \qquad (4)$$
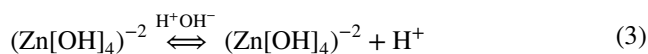
Synthesis of ZnO-EG@DW-based nanofluids with the help of probe sonication

The above presented synthesis describes the use of sono-chemically synthesized ZnO nanoparticles that are physically blended by probe sonication method in a mixture of EG@DW with (50:50) ratio to prepare ZnO-EG@DW-based nanofluids and then run them in a single tube square shaped heat exchanger for to improve the heat transfer. The ZnO nanoparticles were created by using a facile one pot sonochemical method. After synthesis, the ZnO nanoparticles were dispersed in a mixture of EG@DW for 2 h continuously to obtain uniform and homogeneous dispersion without adding any kind of stabilizing agent and surfactant. Four changed (0.1, 0.075, 0.050, and 0.025 mass%) concentrations of the ZnO nanoparticles were dispersed in the EG@DW mixture and highly sonicated by using probe sonication. Also, the 2 h sonication is the preferred duration for equal/uniform ZnO dispersion in the base fluid, so this way dispersion and suspension increase up to three months without using any surfactant. Figure 2a is showing varying base fluids like DW, Ethylene glycol (EG), and a mixture of both DW and EG. The mixture of both EG@DW at (50:50) base fluid was used to prepare the ZnO-EG@DW-based nanofluids at varying mass% concentrations. The 2-step line flow of nanofluids preparation is shown in Fig. 2b, where the first step showing the ZnO synthesis by using one pot sonochemical technique and then were blended in base fluid EG@DW under constant high probe sonication. Finally, the four well dispersed and stable at different (0.1; 0.075; 0.050; and 0.025 mass%) of ZnO-EG@DW-based nanofluids were prepared.

Test section geometry

A square heat exchanger is a design of stainless steel having 1200 mm long and 0.01 m hydraulic diameter from both ends is a significant part of the heat transfer experimental test rig. The heated area of the square heat exchanger was wrapped by electrical insulating tape up to 1200 mm from the start point to end. The maximum delivered power by heater was 600 W capacity; it has been controlled by using voltage regulating supply. A heavy coating of insulating wool was whorled over the square heat exchanger and fully shielded by an aluminum sheet to evade the heat releasing
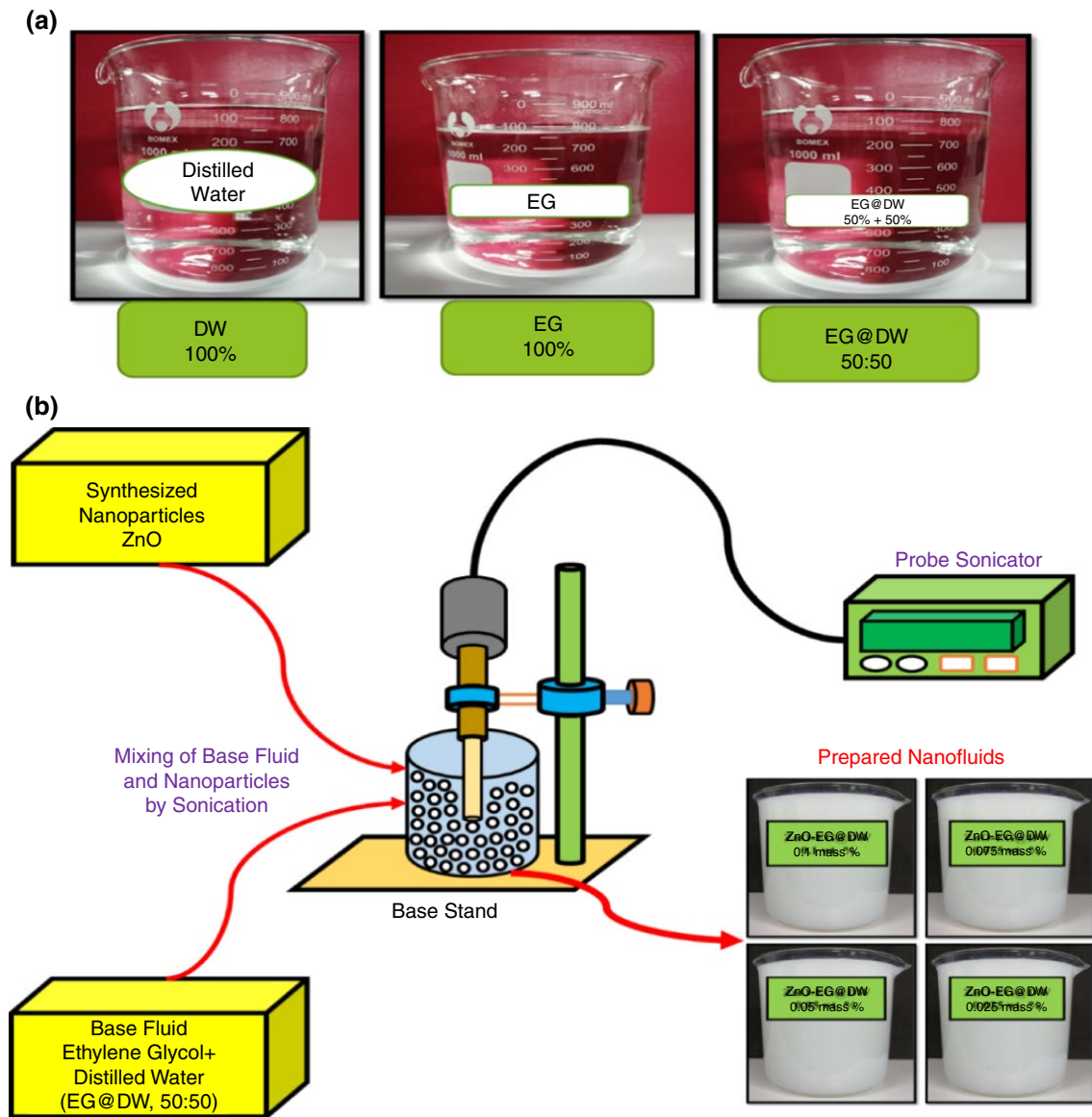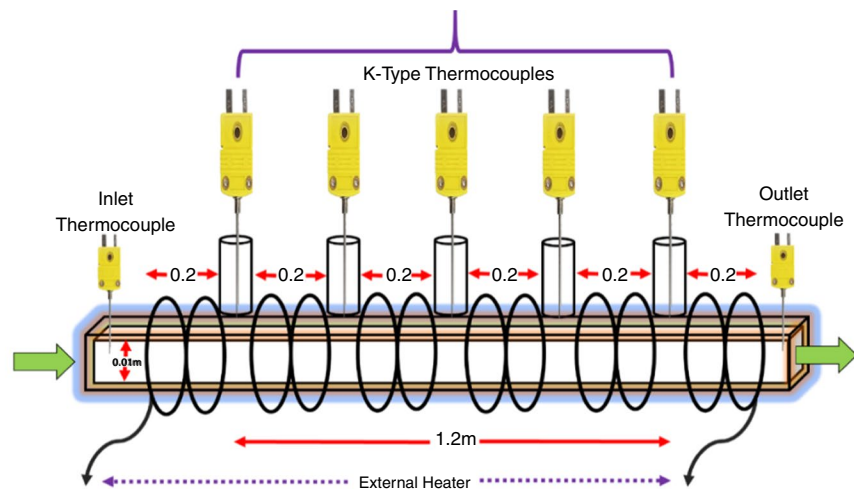

Fig. 1 Synthesis flow of ZnO solid nanoparticles

Fig. 2 **a** Distilled water (100%), Ethylene Glycol (EG-100%), and Ethylene Glycol and Distilled water (EG@DW-50:50), and **b** Two-step line flow for the preparation of ZnO-EG@DW-based nanofluids

by heat exchanger outer surfaces. K-Type five sensitive thermocouples were attached at various points over the surface of the square heat pipe and separated from each other with an equal distance of 0.2 m of the total length as shown in Fig. 3a. Close to the nanofluids flow channel, two additional inlet-outlets, thermocouples were connected with a square heat pipe to enumerate the bulk temperature. Figure 3a is showing the 2-D schematic view and complete insulated (Glass wool) square heat exchanger, while Fig. 3b is showing a pictorial view of the complete heat transfer test rig showing varying parts along with heat exchangers.

Experimental

The experiments were executed over a well designed heat transfer test rig as given in Fig. 4. The test rig includes the main nanofluid flow loop along the different bypass, nanofluid pump, flow meter, inlet–outlet, nanofluid, and fluid tank. Further, the pressure meter, valves for heat exchangers, main valve, pressure gauge, K-type thermocouples, chiller, power supply, data logger GRAPHTECH-GL/220, etc., are also the important parts. The voltage regulator, control panel, frequency control, heater control, and different indicators on the control panel were all separately connected to the setup. All the parts and the square heat exchanger are shown

(a) The 2-D schematic view and complete insulated
(Glass wool) square heat exchanger.

(b) Pictorial view of complete heat transfer test rig showing
varying parts along with heat exchangers.

in Fig. 4 schematic/pictorial diagrams. The nanofluid flow loop starts from the maximum 10L capacity of the fluid tank where the nanofluids were stirred throughout the experiment and a chiller was used to keep the temperature constant. The Araki-EX-70R fluid pump was used to pump the nanofluids with a maximum 88 L/min capacity and all about zero discharge heads. The pump flow was controlled by adjusting frequency at main electric control panel according to the experimental requirement. The PX154-025DI/OMEGA company pressure transducer with an accuracy of ± 0.075% was used to measure the pressure drop during nanofluids running on the test rig. Preceding to start the experiment, the proper arrangement of the heat exchanger and other parameters is the key importance to provide a constant heat flux to outer surface of the square heat exchanger. The five K-type thermocouples are connected at numerous locations alongside the square heat exchanger and to measure the surface temperature by Wilson plot calculations [33, 34].

Additionally, the different thermo-physical characteristics of newly synthesized ZnO-EG@DW nanofluids based were inspected for the improved heat transfer (Nusselt numbers) studies, fluid friction, total overall pressure drop "ΔP" and local or average heat transfer. By using the cooling law of Newton for nanofluids, both inlet–outlet temperatures, bulk temperatures, nanofluid internal temperatures, surface temperature, and the total heat transfer coefficient were calculated. Also, constant heat flux and variable flow rate conditions were followed throughout the experiment. Eight varying flow rate were trailed here in this study.

Thermal conductivity analysis for ZnO-EG@ DW-based nanofluids

Figure 5 displays the KD-2 Pro thermal Analyzer setup of Decagon company to calculate the thermal conductivities of varying ZnO-EG@DW mass% concentrations by employing
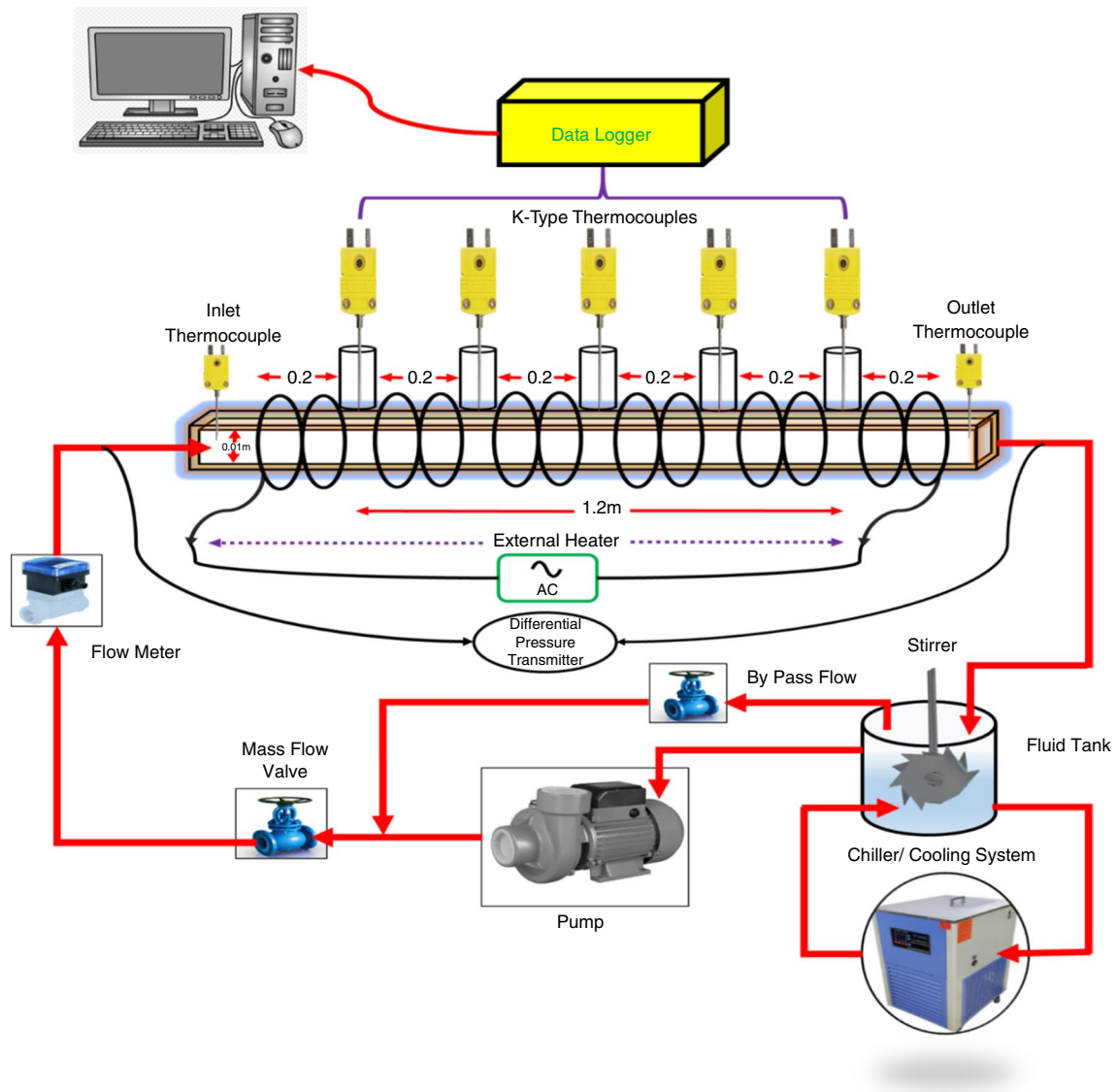
Fig. 4 Complete schematic design of heat transfer test rig along with varying parts

the ASTM/D-5334 and IEEE- 442/1981 standards. The below shown setup of thermal analyzer tracks the transient line heat sources to read the thermal properties of nanofluids. The experiments were executed to analyze the thermal conductivity for ZnO-EG@DW nanofluids with temperature ranges starting from 20 to 45 °C. A cooling system (chiller) was used to keep the surrounding temperature maintained. Before starting the thermal conductivity experiment the needle sensor of the thermal analyzer has confirmed by calculating the thermal conductivity of the glycerin standard sample provided by the company. The intended value for the standard sample was 0.285 W m^{-1} K^{-1} with a precision of ± 0.34%. For ZnO-EG@DW-based nanofluids, the experiment was conducted repeatedly and the average values were considered for each temperature range. The entire thermal

conductivity was measured using advanced KD-2 pro thermal analyzer. The six varying temperature ranges 20, 25, 30, 35, 40 and 45 °C were chosen to see the thermal conductivity variation of all nanofluids against temperature. Further, the obtained thermal conductivities calculations are directed for different time intervals depending upon the surrounding temperature becoming stable before each new calculation at the changed mass% of ZnO-EG@DW nanofluids for different ranges of temperatures. This is important to reduce the faults, which happen during the experiment by heat convection due to temperature changes of sensor needle. The ZnO-EG@DW nanofluids at changing mass% concentrations (0.1, 0.075, 0.05, and 0.025 mass%) were tested here for thermal conductivity measurements.
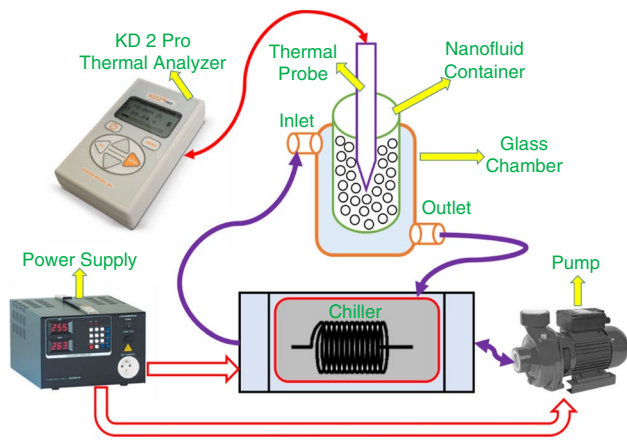
Fig. 5 The KD-2 pro thermal setup for thermal conductivity measurement

Data reduction

The optimal thermal conductivity for ZnO-EG@DW-based nanofluids has been analyzed by use of Maxwell model offered for thermal conductivity [35, 36] as set in Eq. 5 and Eq. 6. Where "k_{eff}" is the overall thermal conductivity, "$\varnothing$" is the volume fraction of the solid nanoparticles, "k_s or k_p" is the thermal conductivity of solid nanoparticles, and "k_f" is the thermal conductivity of the fluid.

$$\frac{keff}{kf} = ks + 2kf + 2\varnothing(kf - ks)/ks + 2kf - \varnothing(kf - ks) \quad (5)$$

$$\frac{keff}{kf} = kp + (n - 1_{kf} - (n - 1)(kf - kp)\varnothing/kp + (n - 1)kf + (kf - kp)\varnothing \quad (6)$$

The average and local heat transfer (h) were evaluated using Eq. 7. Where "q" is known as the value of heat flux, Heat exchanger wall temperature is "Tw" and the bulk temperature is "Tb." The amount of bulk temperature was calculated by following Newton's cooling law.

$$h = \left(\frac{q''}{Tw - Tb} \right) \quad (7)$$

The total delivered power of closed square exchanger and its area was considered to find the value of overall expanded heat flux by the heater. Where "Q" is the power which is the product of both $V \times I$ that has been applied to the heater and similarly the "A" is a dynamical area of the heat exchanger as shown in Eq. 8.

$$q'' = \left(\frac{Q}{A} \right) \quad (8)$$

The square pipe (heat exchanger) area could be calculated by using Eq. 9.

$$A = 4AL \quad (9)$$

where "A" is the area of the square pipe and "L" is the total length of the square heat exchanger.

In the present research, the maximum power delivered to the heat exchanger surface by the heater is 600 W. To find the value of Nu, Eq. 6 was used throughout the experiment, where "h" is known as heat transfer coefficient, "D_h" is known as the hydraulic diameter while "k" defines the entire thermal conductivities. Furthermore, varying empirical correlations that were presented by Petukhov [37], and Gnielinski [38] have been used to calculate Nusselt numbers "Nu" of the single nanofluids. These Nusselt numbers "Nu" could be assessed as well by using Eqs. 10, 12, 13, and 14.

$$Nu = \left(h * \frac{D_h}{K} \right) \quad (10)$$

Equation 11 was used to measure the value of Reynold numbers "Re." Different flow rates were selected and later were converted to velocities. The "ρ" is the overall density of the Nano-fluid, "v" is the value of velocities which is based on flow rates, "μ" is the kinematic and dynamic viscosities of the nanofluids, and "D" is the overall diameter of the heat exchanger.

$$\text{Re} = \left(\frac{\rho v D}{\mu} \right) \quad (11)$$

The Nusselt numbers "Nu" were calculated by using varying empirical correlations offered by Petukhov [37], Dittus-Boelter [39], and Gnielinski [38]. Where "f" is the friction of ZnO nanoparticles flowing inside the heat exchanger, "Pr" is showing the Prandtl numbers and "Re" is the specific Reynold numbers.

$$\text{Nu} = \left(\frac{\left(\frac{f}{8} \right)(\text{Re} - 1000)\,\text{Pr}}{1 + +12.7\left(\frac{f}{8} \right)^{0.5}\left(\text{Pr}^\wedge 2/3 - 1 \right)} \right) \quad (12)$$

$$\text{Nu} = \left(\frac{\left(\frac{f}{8} \right)\text{RePr}}{1.07 + 12.7\left(\frac{f}{8} \right)^{0.5}(\text{Pr}^\wedge 2/3 - 1)} \right) \quad (13)$$

$$\text{Nu} = \left(0.023\,\text{Re}^{0.8}\text{Pr}^0.4 \right) \quad (14)$$

The value of friction coefficient "f" was analyzed inside the square heat exchanger by using Eqs. 15, 16, and 17 that was predicted by Petukhov [37] and Blasius [40]. Equation 12 represents the overall friction loss of the square heat exchanger, whereas "ΔP" is representing the complete pressure drop of the square shaped heat exchanger, "L" is the

heat exchanger total length, "D" is the total diameter "ρ" is showing to the density and "v" denotes velocities inside the square heat exchanger.

$$f = (0.79 \ln \text{Re} - 1.64)^{-2} \tag{15}$$

$$f = \frac{\Delta P}{\left(\frac{L}{D}\right)\left(\frac{\rho v^2}{2}\right)} \tag{16}$$

$$f = 0.3164re^{-0.25} \tag{17}$$

Equation 18 and Eq. 19 were used to calculate the required pumping power of the square shaped heat exchanger. Equation 18 can be mainly used when the Reynolds numbers "Re" are constant. Therefore, "ρ" is the density of nanofluids, "D" is the diameter of the square heat exchanger, "μ" is the viscosity of the Nano-fluids, "ρ_{bf}" is the base fluid density, "ρbf" is the Nano-fluids density, "μ_{bf}" is the base fluid viscosity and "μ_{nf}" is the Nano-fluids viscosity.

$$W = 0.158\left(\frac{4}{\pi}\right)^{1.75}\left(\frac{Lm^{2.75}\mu^{0.25}}{\rho^2 D^{4.75}}\right) \tag{18}$$

$$\frac{\text{Wnf}}{\text{Wbf}} = \left(\frac{\rho bf}{\rho nf}\right)^2\left(\frac{\mu nf}{\mu bf}\right)^3 \tag{19}$$

Characterizations of ZnO-EG@DW-based stable nanofluids

The optical behavior and energy band gaps of ZnO particles were examined by using a UV–Vis spectrum analyzer (UV 1800 Shimadzu corp 08,579). The absorbance level at all mass% of newly Sonochemically synthesized ZnO-EG@DW nanofluids as a function of energies band gaps (E_g) from pH level 8–11 has been recorded by UV–Vis spectrum analyzer. The absorbance level in % could resolute by UV–Vis spectrum analyzer and (hv) was calculated by equating wavelength λ where h$v = h*c/\lambda$, where "h" is the Planck constant (6.62×10^{-34}), λ = total wavelength 800–200 nm c = light speed 3×10^8 in m/s [41]. The morphological erection of the sonochemically synthesized ZnO was calculated using XRD analysis (Bruker Advanced X-rays D8 Solutions). The XRD results obtained have matched the (JCPDS) X-ray data files. The crystalline size of ZnO nanoparticles was achieved by calculating the expansion of the different XRD peaks with the desired positioning by using the Scherer formula:

$$LC = \frac{180}{\pi} * k.\frac{\lambda}{\text{Cos}}\emptyset\sqrt{\text{FWHM}^2}.s^2 \tag{20}$$

Where π is equal to 3.142, λ is the wavelength of Cu/K$_\alpha$ radiations and κ is the constant of the Scherer rate (0.89), s is broadening of the instrument (0), while (FWHM) is known as the full width half/maximum of the surface plane (101), and plan angle is θ (101). The FWHM and plane angle have been directly taken out from the (EVA) software, and analyzed by XRD [42].

The FESEM investigation was engaged to see the morphology (Shape) and size of ZnO nanoparticles in presence of different elements by (EDX mapping using Zeiss-Supra 35-VP) energy dispersion X-rays spectrometer. Further, the investigation for attached functional groups with ZnO material was carried out by using FTIR analysis. This analysis was verified by using FTIR spectrum analyzer Perkin Elmer with a range from 4000 to 400 cm^{-1} [6].

UV–Vis spectrum analysis

UV–Vis spectra analysis is the most important and extensively used method for the confirmation of different nanoparticles. The absorbance spectrum of Sonochemically synthesized ZnO nanoparticles has been tested within the specific range of wavelengths from 200 to 800 nm by using a UV-1800 SHIMADZU crop spectrometer with a cuvette length of 10 mm maximum, 190–110 nm minimum, and maximum wavelength capacity [43]. UV–Vis spectra test was executed to notice the optical conduct for Sonochemically produced ZnO. All the ZnO particles displayed a robust absorption level at 376 nm, which is dependent onto blue-lateral shifting of ZnO nanoparticles in bulk as given in Fig. 6. The UV–Vis spectrum analysis for Sonochemically synthesized ZnO nanoparticles has been carried out at 0.05 mass% concentration of nanoparticles in the base fluid, where the prominent peak at 376 nm confirms the ZnO synthesis. Figure 7 shows the absorption levels at four changing (0.1, 0.075, 0.05, and 0.025 mass%) of ZnO-EG@DW type nanofluids, where it can be seen that the absorbance level is increased with an increase in mass% concentration of the solid nanoparticles into base fluid [44, 45].

Figure 7 describes the maximum absorption level of the Sonochemically synthesized ZnO-EG@DW nanofluids at varying mass% (0.1, 0.075, 0.05, and 0.025) concentrations at normal temperature. The noticeable peak at 372 nm at varying mass% of ZnO-EG@DW reveals the confirmed preparation of ZnO particles by using probe sonication method. Consequently changed (0.1, 0.075, 0.05, and 0.025 mass%) of ZnO-EG@DW nanofluids display the different absorption levels due to the presence of maximum solid ZnO in the base fluid, where it can see a rise in mass% of ZnO increased the absorption level. The maximum absorption of 2.8% was observed at 0.1 mass% concentration of the ZnO-EG@DW-based nanofluids.
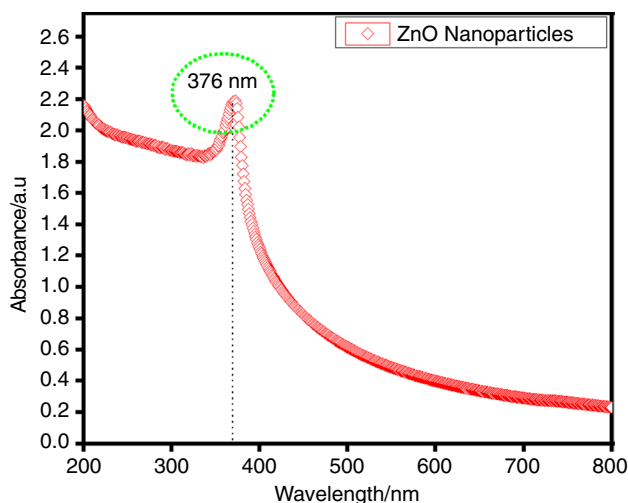
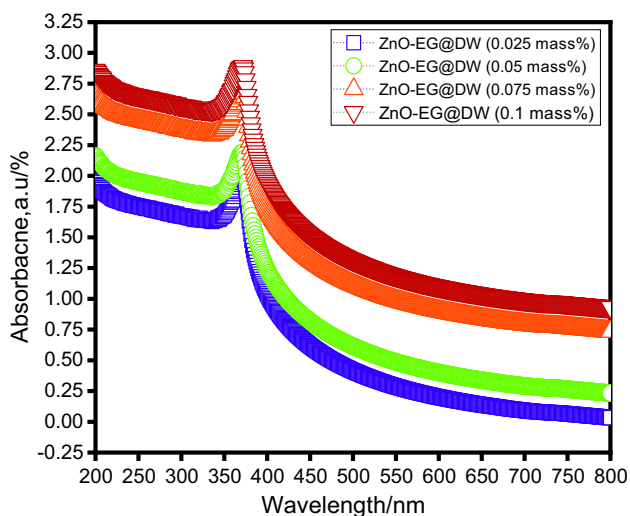**Fig. 6** The UV–Vis spectrum of ZnO nanoparticles

Fig. 7 UV–Vis spectrum analysis for absorbance ratio of ZnO-EG@DW-based nanofluids mass%

XRD investigation

The XRD of sonochemically synthesized ZnO nanoparticles was conducted at Makmal Sinaran-X, University Malaya 301, Aras#1, Bangunan Utama (J-22), Jabatan Geologi by using apparatus of Malvern Analytical Model: EMPYREAN. The white color ZnO nanoparticles were synthesized by adopting a one-pot sonochemical-assisted method where a pH of 11 was considered to produce crystalline nanoparticles. Figure 8 describes the X-ray diffraction spectra of sonochemically synthesized ZnO nanoparticles for nanofluids prepared with a pH value of 11. The ZnO nanoparticles cannot be synthesized very well with pH value 6 because of their low concentrations of OH^- ions and H^+ ions in the

solution. Chand, P. et al. [46] describe that the ZnO nanoparticles having $pH \geq 8$ give the crystalline nature of the nanoparticles with different diffraction angles of 2θ. The three different prominent peaks are considered to be the 100, 002, and 101 correspondingly to the planes. The 101 peak is to consider the preferred orientation of ZnO nanoparticles with ≥ 8 pH values. The maximum intensity peak for ZnO nanoparticles was noticed at pH 11 due to enough presence of OH^- ions to formulate the ZnO nanoparticles. All the detected peaks with pH 11 show the successful synthesis of ZnO nanoparticles and all the bases and precursors are fully decomposed and no impurity has been found during the X-ray-diffraction analysis.

FTIR analysis

The one-pot facile sonochemical synthesis method was used to synthesis the ZnO nanoparticles where the pH level was adjusted at 11 to obtain the crystalline nanoparticles with specific morphology. Figure 9 displays the Fourier transform infrared (FTIR) spectrum of sonochemically synthesized ZnO nanoparticles with pH 11. Fernandes D. et al. [47] explain that the energy bands from 3543 to 3393 cm^{-1} correspond to the vibration mode for O and H. When the pH increased the O and H peaks became narrower due to the additional presence of O and H ions from NaOH which strongly reacts with the zinc acetate precursor solution at higher pH values. The maximum vibration and stretch mode has been observed between 1420 and 1570 cm^{-1}. The symmetrical vibration and stretching occur between 1450 and 1330 cm^{-1} due to the presence of C and O. The prominent peaks of ZnO nanoparticles that appear between 550 and 400 cm^{-1} ranges describe that $Zn(OH)_2$ are completely transformed into ZnO nanoparticles. So, the nanoparticle
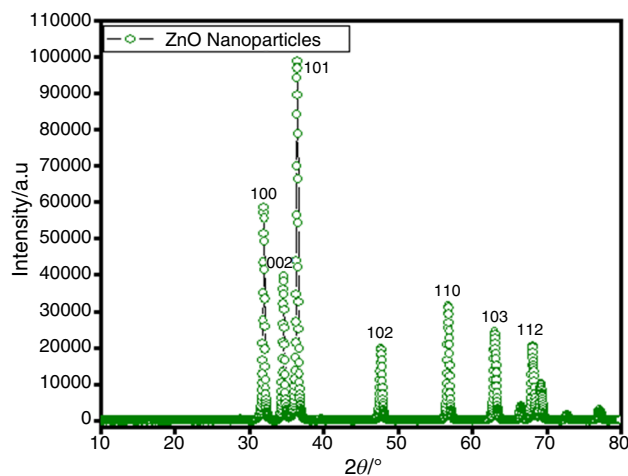

Fig. 8 The X-ray diffraction (XRD) spectra of Sonochemically synthesized ZnO nanoparticles
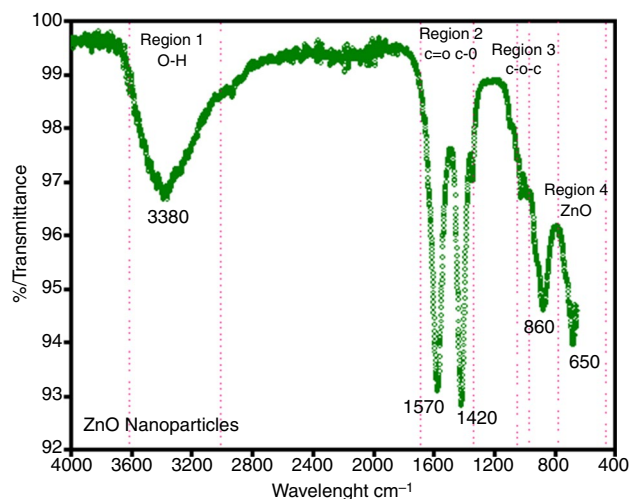
Fig. 9 The Fourier transforms infrared spectroscopy (FTIR) ZnO nanoparticles

Fig. 10 FESEM analysis showing the ZnO morphology

size affects the shifting rate of peaks due to which FTIR aid FESEM images [48].

FESEM analysis

Figure 10 displays the FESEM image of Sonochemically produced ZnO nanoparticles. The FESEM image of ZnO nanoparticles displays the homogeneous structure when the pH value raises to alkaline conditions 10 and 11. It can be seen from the FESEM image that most of the ZnO nanoparticles were spherical, where this synthesis technique gives ZnO particles less agglomeration. This low agglomeration happens due to the high centrifuge for washing of the sample at the end. The high-speed centrifuge removes the impurities like hydroxyl ions and increases the interaction between Zn and O ions [49]. Where the OH^- ions aid the nucleation process and growth of the formation of ZnO nanoparticles, and the increase in pH value up to 10 and 11 the particle size decreased [50]. Smaller ZnO particle size is helpful for ZnO-EG@DW-based nanofluids dispersion and can enhance the heat transfer properties.

Results and discussion

We executed the experiments in different stages. 1. In the first stage, we used a single pot sonochemical synthesis technique including (Chemical reaction, sonication, drying, centrifuge, and calcination) to produce ZnO nanoparticles in bulk. 2. In the second stage, we have done the necessary characterizations to see the proper ZnO synthesis. 3. In the third stage, we prepared ZnO-EG@DW nanofluids
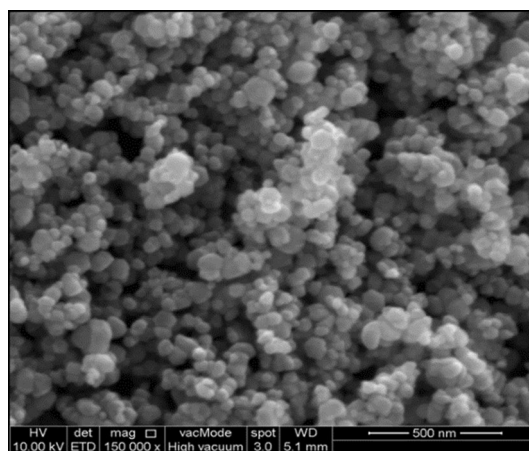
by following a two-step technique. 4. In the fourth stage, all thermo-physical characteristics like dynamic/kinematic viscosities, densities and thermal conductivity, were tested. 5. In the final stage, our targeted properties including stability/dispersion, thermal properties, and hydrodynamic characteristics like (Heat transfer coefficient "h," Nusselt Numbers "Nu," Friction loss, pressure drop, and required pumping power) were investigated in detail.

For the thermal and hydrodynamic characteristics, the steady heat flux and changing flow conditions were used. Eight varying flow rates were considered to see the consequence of heat transfer improvement in square shaped heat exchanger geometry. Also, their hydrodynamics effects were calculated accordingly. Finally, the outcomes were equated with previously presented varying correlations that showed an association.

Dispersion and stability of ZnO-EG@DW-based nanofluids

The different thermophysical properties of ZnO-EG@DW nanofluids are extremely affected by their stability and dispersion in the EG@DW. Similarly, as stated in the literature, a maximum dispersion and stability of around 4–6 weeks have been reported for ZnO-based nanofluids, where different surfactants and dispersants were used to escalate the solid nanoparticles stability and longer suspension [49–51]. The current study emphasizes to improve the stability and dispersion of the ZnO-EG@DW-based Nano-fluids without using surfactant. Stability represents the aggregate of suspended particles at a significant rate. Particles in the dispersion may adhere together and form aggregates of increasing size which may settle out due to gravity. The rate of aggregation is in general determined by

the frequency of collisions and the probability of cohesion during collision. In fact, the stability of a particle in solution is determined by the sum of van der Waals attractive and electrical double layer repulsive forces which endures between particles as they approach each other due to the Brownian motion [51, 52]. At a large attractive force, the particles collide and make unstable suspension. At sufficiently high repulsion of particles, the suspensions remain in a stable state. Thus, with the dominated repulsive forces between particles nanofluids or colloids could be stable. Two types (steric, electrostatic) or repulsive forces are recognized [53].

Figure 11a and b is presenting the physical observation and stability graph obtained by UV–Vis spectroscopy of Sonochemically dispersed ZnO-EG@DW-based nanofluids at varying (0.1, 0.075, 0.05, and 0.025 mass%) concentrations. No sedimentation occurred for stated nanofluids for 3 months after the preparation for all mass% concentrations. This longer dispersion is mainly accredited to a smaller size, the viscosity of the base fluid (EG@DW), and sonication time during preparation. Figure 11a reveals the reliability of ZnO nanoparticles dispersion and stability in the EG@DW mixture exposed to high Probe sonication for (0.1, 0.075, 0.05, and 0.025 mass%) of ZnO-EG@DW-based nanofluids. The sonicator setting was made according to (Total I/P voltage 220 v, Frequency 20 kHz, Pulse Amp 80, Pulse duration 3–2 s on and off, total delivered energy 36000 J, Probe Temp 0 °C, Total Power 750 W) has been adjusted for the probe sonication of ZnO-EG@DW-based nanofluids for 2 h continuously. The pictorial images in Fig. 11b display the uniform dispersion of ZnO nanoparticles in the EG@DW mixture and look very stable until 11 weeks for all the mass% concentrations after their preparation and nanoparticles are well dispersed in EG@DW without any surfactant. Sonication time increases the dispersion of ZnO nanoparticles in base fluid due to which it becomes stable. From week 11 to onward all the sample starts from fewer sediments and high sedimentation was noticed for 0.025% sample because of lower amounts of ZnO nanoparticles. Figure 11c is expressing the comparison of ZnO-EG@DW-based nanofluids at 0.1 mass% concentration before use and after use after the day of preparation for equal time slots of (30, 60, and 90) days to check their stable characteristics for heat transfer studies. The UV–Vis analysis was conducted to check the behavior of ZnO-EG@DW nanofluids with different time passages like (on the day of preparation, after (30 days, 60 days, and finally after 90 days). It can be seen in Fig. 11c that the absorbance % and the prominent peak at 288 nm are stable for all sonication time, which is the strong justification that the nanofluids didn't lose its properties even before and after the use. Therefore, the same nanofluids easily could be re-used by again sonication.

Thermophysical characteristics of ZnO-EG@DW nanofluids

Figure 12a displays the thermal conductivity enrichment for the ZnO-EG@DW-based nanofluids at changed (0.1, 0.075, 0.05, 0.025 mass%) concentrations at numerous temperatures ranges from 20 to 45 °C. The thermal conductivity of all the mass% of ZnO-EG@DW nanofluids exhibited growing trends with an increase in temperature value, which has already an agreement in earlier researches [54, 55], whereas the EG@DW displays declining trends with an increase in temperature. The same declining behavior has already been reported in earlier experiments steered by Asadi et al. [55, 56] and Aberomand et al. [57]. The mounting inclination has been detected at all mass% of ZnO-EG@DW nanofluids. An linear surge in ZnO particles collisions and their Brownian motions could be the obvious key reason for enhancing the overall thermal conductivity of ZnO-EG@DW nanofluids with a temperature change. The thermal behavior of the ZnO-EG@DW nanofluids with different mass% concentrations is shown in Fig. 12a. where the thermal conductivities of all mass% of ZnO-EG@DW nanofluids present a growing trend as the mass% concentration increases. This growing trend was noticed for all the temperature values. Also, the graph shows the addition of ZnO in EG@DW led to an improvement in the thermal conductivity of the base fluid, which was previously reported by several researchers. So the use of these nanofluids/Nano-coolants with solid mass% concentrations could be commended for different cooling applications.

The dynamic viscosity of EG@DW and ZnO-EG@DW nanofluids moderates with the rise in temperature of the fluid, and the viscosity outcomes for all (0.1, 0.075, 0.05, and 0.025) mass% of ZnO-EG@DW nanofluids and EG@DW as well against different mass% of ZnO nanoparticles are given in Fig. 12b. The key reason for this increasing behavior of viscosity value is due to an increase in mass% of particles in base fluid (EG@DW) while the viscosity ratio for all mass% exhibits the declining trend against the increase in temperature value. This declining behavior of the viscosity of ZnO-EG@DW type nanofluids is due to their weak internal molecular interaction force [58, 59]. The detailed dynamic viscosities at all concentrations of ZnO-EG@DW type nanofluids and EG@DW base are illustrated in Table 1, where the observed minimum and maximum temperature range was from 20 to 45 °C. Similarly, Fig. 12c shows the same declining trend for the kinematic viscosity of EG@DW and varying concentrations of ZnO-EG@DW type nanofluids against the temperature values. While the increase in viscosities value is due to the increase in mass% of ZnO solid nanoparticles in the base fluid EG@DW. The 0.1 concentration of the ZnO-EG@DW showed highly dynamic and kinematic viscosities due to the existence of
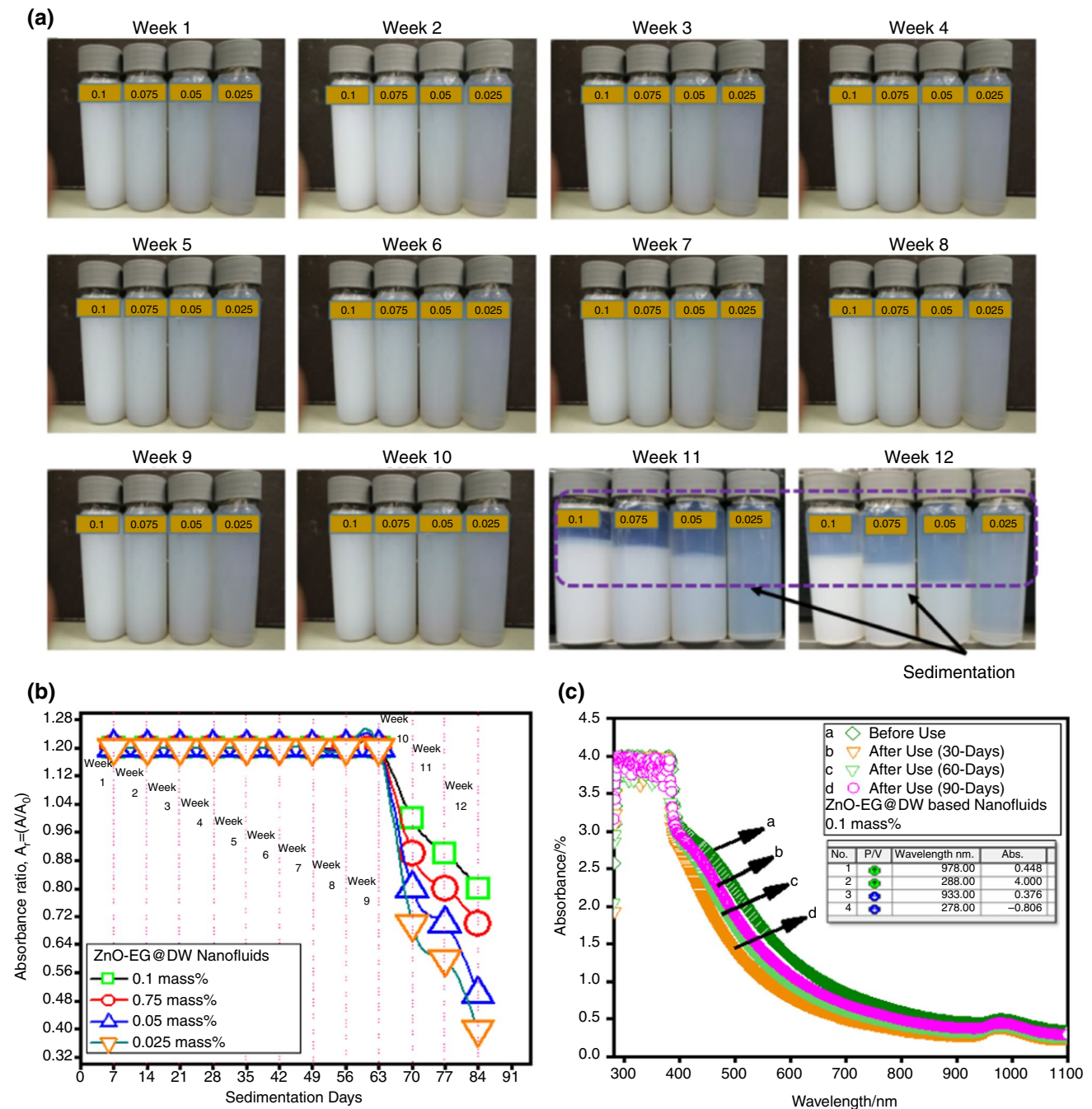
(a)

(b)   **(c)**

Fig. 11 **a** ZnO sedimentation effecting to the dispersion and stability of the nanofluids, **b** Dispersion and stability behavior for ZnO-EG@DW nanofluids, **c** UV–Vis showing the stable characteristics of ZnO-EG@DW-based Nano-fluids after and before use on test rig

the maximum concentration of ZnO in EG@DW. The behavior of all mass% concentrations of the ZnO-EG@DW-based nanofluids and base fluid EG@DW against the temperature variations are given in Table. 2.

Figure 12d shows the density behavior of EG@DW and varying concentrations of ZnO-EG@DW-based nanofluids.

After adding the ZnO nanoparticles to EG@DW, the overall density of the nanofluids has changed according to mass% of nanoparticles. Also, due to an increase in the temperature value the density of all fluids starts to decrease slightly. When the temperature was low, all fluids showed maximum density, the maximum density was noticed for
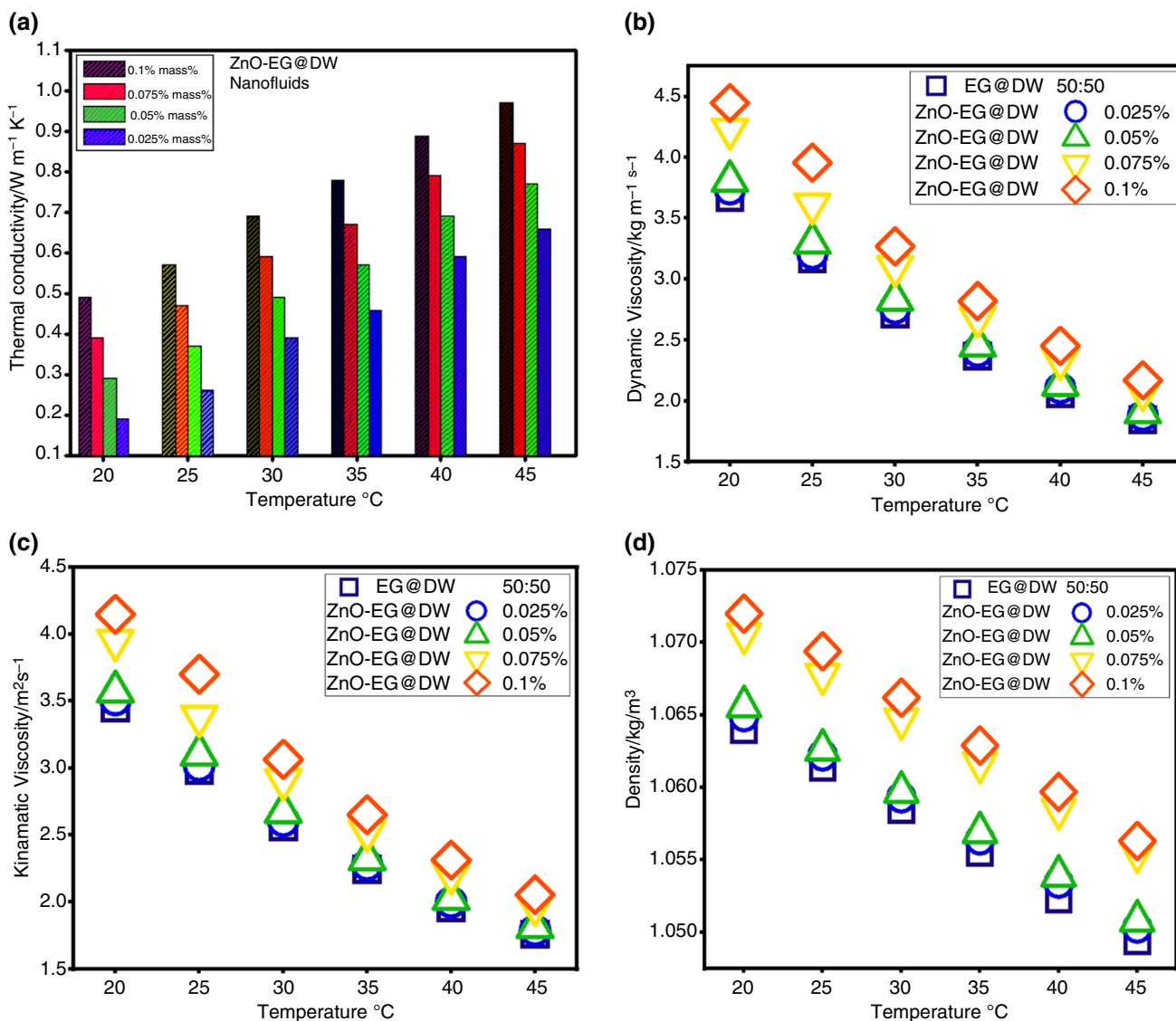
Fig. 12 **a** Variations in thermal conductivities for at varying ZnO-EG@DW mass%., **b** Dynamic viscosity variations against varying temperatures at varying mass% of the ZnO-EG@DW nanofluids, **c** Kinematic viscosity variations against varying temperatures for changed concentrations of the ZnO-EG@DW nanofluids, and **d** Density behavior against the varying temperatures of the EG@DW mixture and all concentrations of ZnO-EG@DW-based nanofluids

Table 1 Dynamic viscosity profile at varying concentrations of ZnO-EG@DW-based nanofluids and EG@DW mixture

Temp	0.025\ mass%	0.05\ mass%	0.075\ mass%	0.1\ mass%	EG@DW 50:50
20	3.8066	3.6669	3.7345	4.2306	4.4475
25	3.2956	3.1650	3.2054	3.6158	3.9572
30	2.8319	2.7125	2.758	3.1027	3.2682
35	2.4524	2.3668	2.4038	2.6871	2.8195
40	2.1311	2.0572	2.1034	2.3398	2.4516
45	1.9038	1.8447	1.8763	2.0841	2.1699

Table 2 Kinematic viscosity profile at all concentrations of ZnO-EG@DW-based nanofluids and EG@DW mixture

Temp	0.025/ mass%	0.05/ mass%	0.075/ mass%	0.1/ mass%	EG@DW50:50
20	3.5722	3.4462	3.5069	3.9514	4.1488
25	3.1014	2.982	3.0177	3.3862	3.7005
30	2.6723	2.5626	2.6035	2.9141	3.0653
35	2.3203	2.2424	2.2755	2.5310	2.6525
40	2.0222	1.9549	1.9968	2.2105	2.3136
45	1.8118	1.7579	1.7864	1.9745	2.0541

higher concentration of the ZnO-EG@DW-based nanofluids. Though the EG@DW and the lowest concentration of ZnO-EG@DW-based nanofluids showed lower density as compared to other fluids, these density variations are credited to the occurrence of the ZnO. The detailed density behavior of all mass% concentrations of the ZnO-EG@DW-based nanofluids and base fluid EG@DW for different values of temperature is shown in Table3.

Hydrodynamic characteristics of all concentrations of ZnO-EG@DW-based nanofluids inside a square heat exchanger

To study the total pressure drop inside the square heat exchanger, we intended the friction factor for EG@DW mixture and all concentrations of ZnO-EG@DW-based nanofluids, respectively. In the current study, the results that

arise from the calculation of the friction factor in Fig. 13a, where the outcomes show a falling trend with a growth in Reynolds numbers, all concentrations showed a decrease in friction factor due to an increase in velocity which affects the Reynolds increase. The friction was evaluated considering the overall pressure drop "ΔP," length of the heat exchanger "L," hydraulic diameter of the heat exchanger "D," viscosity "V," and density "ρ" of the running fluid. To calculate the changes in pressure drop across square heat exchanger, calculations have been done to find the friction loss for base fluid in the square heat exchanger by applying Eq. 16. The assessed results were compared with Blasius's [40] and Petukhov model [60] Models where the total difference was

$$< \tag{21}$$

5% when it has compared with Blasius and Petukhov correlations results. These correlations showed that the square shaped heat exchanger is reliable to notice the total pressure drop across the test section for changed Reynolds values stated in the research. The entire pressure drop across the square shaped heat exchanger of ZnO-EG@DW-based nanofluids at different concentrations according to Reynolds (Re) is given in Fig. 13b. During the experiment, it has been observed that there is a slight surge in pressure drop of ZnO-EG@DW nanofluids as in comparison to EG@DW. This increase in pressure drop was reported due to the existence of ZnO in EG@DW, which may increase the friction loss resulting in an increase in the overall pressure drop.
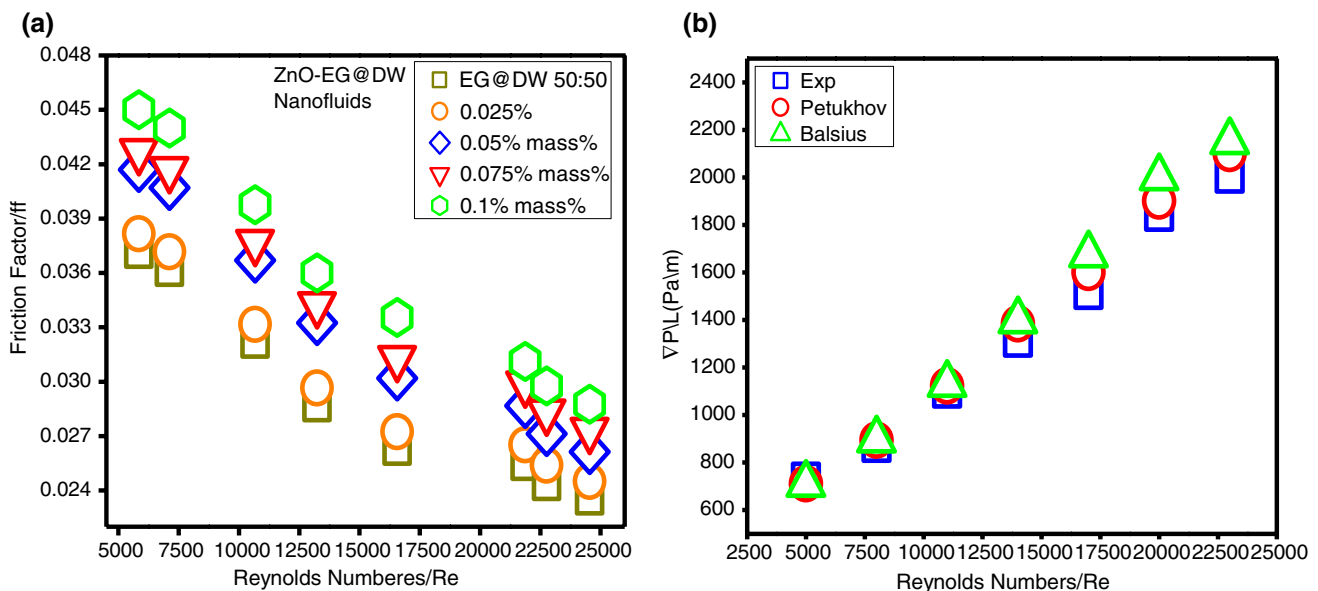
Table 3 Densities of all concentrations of ZnO-EG@DW-based nanofluids and EG@DW mixture

Temp	0.025/ mass%	0.05/ mass%	0.075/ mass%	0.1/ mass%	EG@DW 50:50
20	1.0656	1.0640	1.0649	1.0706	1.072
25	1.0626	1.0614	1.0622	1.0678	1.0694
30	1.0597	1.0585	1.0593	1.0647	1.0662
35	1.0569	1.0555	1.0564	1.0617	1.0629
40	1.0539	1.0523	1.0534	1.0585	1.0597
45	1.0508	1.0494	1.0503	1.0555	1.0563

Fig. 13 **a** Comparison of friction loss of ZnO-EG@DW nanofluids and EG@DW, **b** Comparison of experimental and model data between pressure drop and Reynolds numbers

Average heat transfer (h) and average Nusselt (Nu) numbers analysis of all concentrations of ZnO-EG@DW-based nanofluids

Detailed investigations describe the positive effects varying mass% concentrations(0.1, 0.075, 0.05, and 0.025) of ZnO-EG@DW-based nanofluids on average heat transfer/Nusselt numbers for specified Reynolds ranging from 4550 to 20,360. The changing flow value and persistent heat flux conditions were chosen throughout the experiment. The experimental process has been conducted to assess the average heat transfer (h) and their special effects on to average Nusselt (Nu) numbers in the square shaped heat exchanger of ZnO-EG@DW-based nanofluids. The calibration and necessary setting of the heat transfer experimental setup was maintained on a priority basis before running the experiment. To realize the overall temperature of the heat exchanger surface and its heat conduction at wall of the heat exchanger, as well as the heat convection allowed by ZnO-EG@DW-based nanofluids were studied here. Wilson plot [33] procedure was trailed here, by figuring the resistance at the various locations of the square heat exchanger, also heat transfer in the square heat exchanger. We measured the thermo-physical characteristics of distilled water and varying mass% concentrations of ZnO-EG@DW nanofluids by seeing numerous factors like friction, pumping power, heat transfer (h), pressure drop and Nusselt (Nu) numbers, etc. Likewise, the average heat transfer was recorded for ZnO-EG@DW-based nanofluids running in a square heat exchanger. Figure 14a is describing the typical heat transfer for EG@DW mixture and all concentrations of ZnO-EG@DW-based nanofluids. Further, the growing trend shows an improvement in the heat transfer of at varying concentrations of ZnO-EG@DW nanofluids, although the base fluid (EG@DW) bounces lesser heat transfer coefficient (h) which is credited to the nonexistence of ZnO particles in the EG@DW mixture. Also, it can be seen, the highest enhancement in average value of heat transfer was perceived for at 0.1 concentration of ZnO-EG@DW-based nanofluids which are nearly about to 600–1800 W m^{-1} K^{-1}, similarly rest all mass% concentrations showed improved heat transfer outcomes compared to EG@DW mixture but less enhanced than 0.1 mass% concentration. The outcomes accomplish the full existence of ZnO particles in base will surge to the heat transfer as well as Reynolds increased.

Figure 14b is presenting a comparison between the current study on heat transfer improvement and the past studies, where different metal oxides were used in different base fluids. The Reynold range was considered within 400 to 25,000. It can be seen in Fig. 14b the use of ZnO in EG@DW mixture is leading to improved heat transfer. This improvement is mainly due to good stability, High flow rate, and higher mass% concentration of the ZnO-EG@DW-based nanofluids.

Based on heat transfer coefficient (h) measurements it's easier to evaluate average Nusselt (Nu) development at all (0.1, 0.075, 0.05, and 0.025 mass%) concentrations of ZnO-EG@DW-based nanofluids. Similarly, Fig. 14c is presenting the increase in average Nusselt (Nu) at all concentrations of ZnO-EG@DW nanofluids with growth Reynolds values varying from 4550 to 20,367. Average Nusselt enhancement for EG@DW is comparatively less than ZnO-EG@DW-based nanofluids, where 0.1 mass% gives the highest improvement against the Reynolds increases. The enhancement of Nusselt numbers relies on the heat transfer coefficient, which mainly increases due to the occurrence of ZnO. After adding the ZnO nanoparticles in the EG@DW the improvement in the Nusselt (Nu) numbers was observed, which has been attributed to the increase in ZnO particles mass%. Also, the enrichment in Nusselt numbers is credited to the increase in Reynolds values, as the Reynolds increasing the average Nusselt numbers were increased accordingly.

The outcomes arising from experimental data were compared with some empirical correlations data, like Petukhov, Gnielinski, and Dittus to find the improvement in average Nusselt numbers of the ZnO-EG@DW-based nanofluids. These empirical correlations are mentioned in Eq. 6 and 7 as well, also these correlations can be used for only the turbulent type flow of the nanofluids. Figure 14d shows the comparison graph of experimental data with correlations data, where the mounting trends in average Nusselt numbers with variation in Reynolds. Also, the experimental results show positive results compared with different model empirical correlations. Therefore, the presented experimental study and setup can be used to study the heat transfer characteristics of the ZnO-EG@DW nanofluids in square heat exchangers.

Local heat transfer coefficient (h)/local Nusselt (Nu) numbers measurement of ZnO-EG@DW-based well stable nanofluids in a square shaped heat exchanger

For the heat transfer measurements at varying points of the square shape heat exchanger (local heat transfer, h) the heat exchanger was calibrated with five K-type sensitive thermocouples on its outer surface. These thermocouples were placed apart from each other at a distance of 0.2 m along the square heat exchanger to measure the local heat transfer values at every point. The investigation was conducted to quantify the effects of ZnO-EG@DW nanofluids with (0.1, 0.075, 0.05, and 0.025) mass% on local heat transfer (h) in the square test section individually. The local heat transfer measurement for all mass% concentrations on five different points of the square heat exchanger has been conducted at
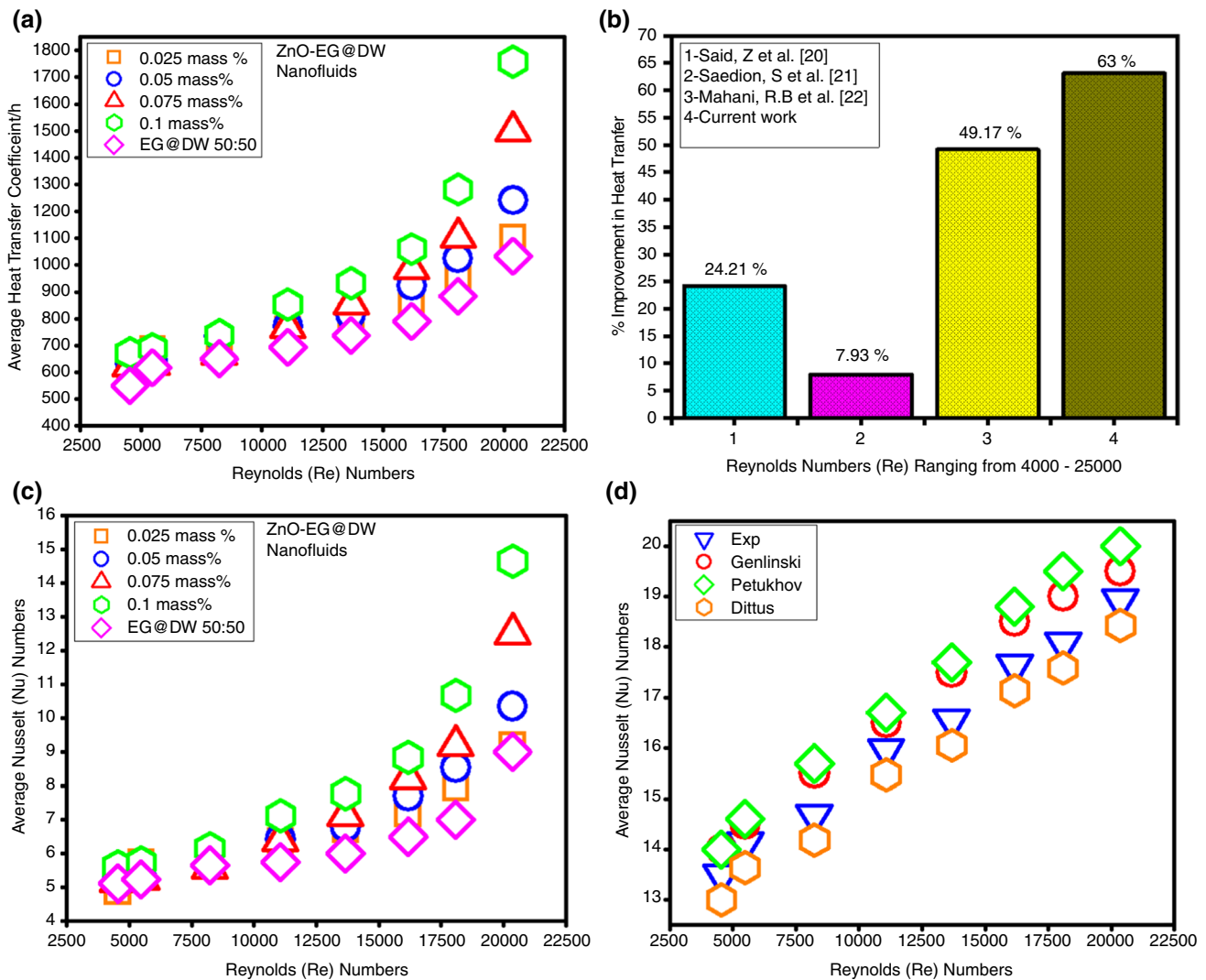
Fig. 14 **a** Average heat transfer development in ZnO-EG@DW nanofluids with changed mass%., **b** Comparison of heat transfer improvement in % of the current study with past, **c** Growth in Nusselt numbers vs Reynolds numbers of the ZnO-EG@DW-based nanofluids, and **d** Comparison between experimental and varying model data results

constant heat flux and changing flow rate settings throughout the experiment. Figure 15a–d indicates the local conduct of the heat transfer (h) for all mass% of ZnO-EG@DW nanofluids at various points of the square test section. All the mass% concentrations were treated individually in a heat exchanger with numerous flow rates or specified range 4550–20,367 of Reynolds were also exposed. Through the experiment, the outcome arises that at the 0.025 mass% of ZnO-EG@DW-based nanofluids exhibited low local heat transfer (h) which is 550–1500 W m^{-2} K^{-1} for Reynolds increasing from 4550 to 20,367. In the case of 0.05 mass% of ZnO-EG@DW nanofluids, the local heat transfer (h) was observed at 550 to 1750 W m^{-2} K^{-1} at identical Reynolds numbers. The 0.075 mass% of ZnO-EG@DW nanofluids show the heat transfer (h) 550–2170 W m^{-2} K^{-1} against the same

Reynolds numbers. Finally, the maximum improvement in local heat transfer was observed at about 550 to 2830 W m^{-2} K^{-1} for the 0.1 mass% of ZnO-EG@DW nanofluids against the same Reynolds values ranging from 4550 to 20,367. At all mass% of the ZnO-EG@DW-based nanofluids exhibited a supreme heat transfer (h) value at the first point of the heat exchanger which is closest to the inlet point of the test section. As the distance increases from the inlet point, the heat transfer decreases according to different flow rates and their respected Reynolds. The supposition from the stated research describes that the presence of ZnO nanoparticles in EG@DW 50:50 and their different mass% addition up to 0.1 mass% exposed to positive growth in local heat transfer coefficient (h) in square heat exchangers.
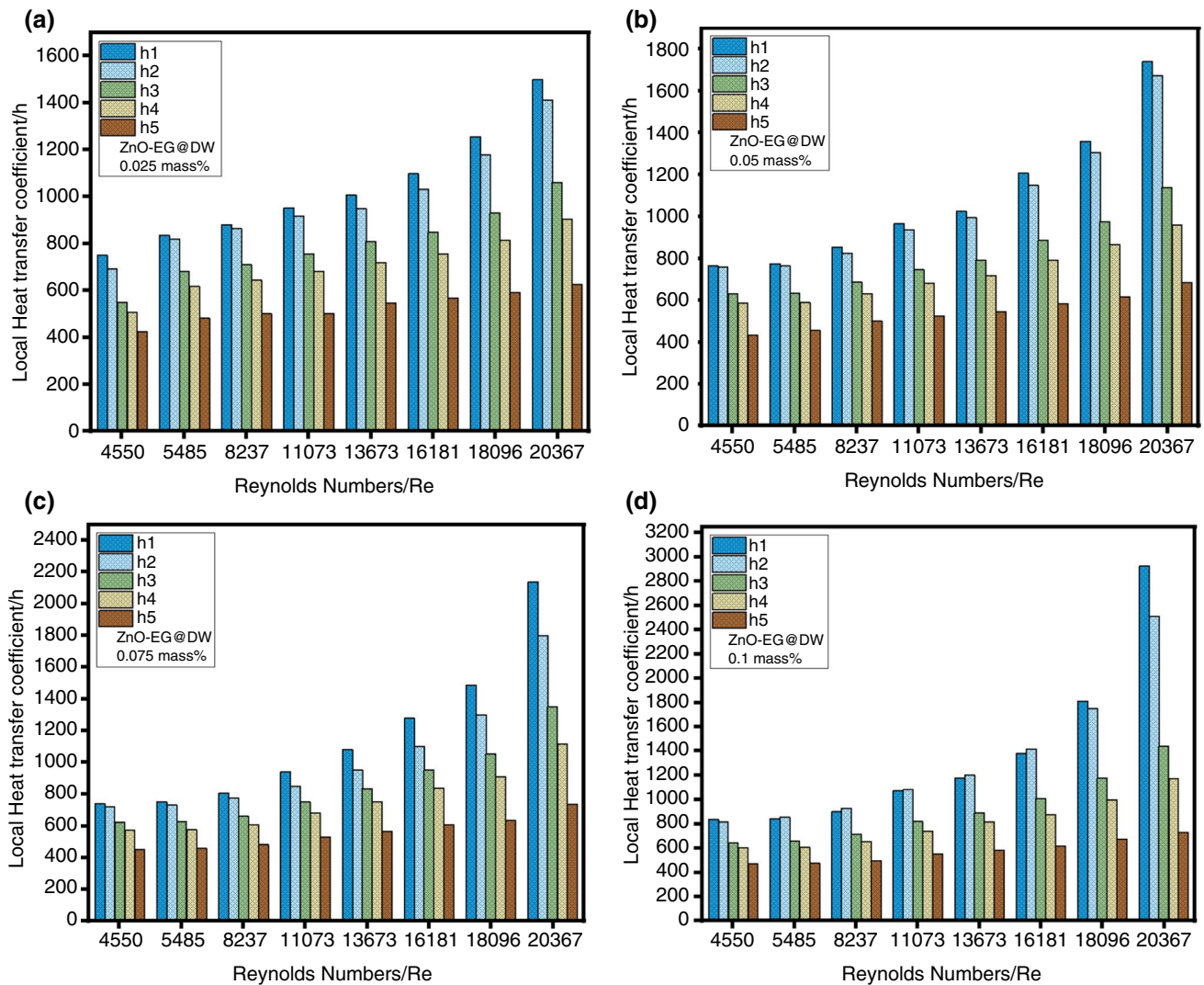
Fig. 15 a-d Variations in local heat transfer coefficient (h) augmentation for all mass% of ZnO-EG@DW-based nanofluids

According to local heat transfer (h) measurements of changing mass% of ZnO-EG@DW-based nanofluids, it is quite easy to calculate the variations in local Nusselt (Nu) on different points alongside the square heat exchanger. Based on heat transfer results, the local Nusselt numbers improvement was assessed for changing mass% of ZnO-EG@DW-based nanofluids accordingly. Figure 16a-d demonstrates the different trends of Nusselt (Nu) for specified Reynolds ranging from 4550 to 20,367 at all mass% like (0.1, 0.075, 0.05, and 0.025) of the ZnO-EG@DW-based nanofluids. Through the experiment, it was observed local Nusselt (Nu) improves with an increase in Reynolds with the same hydraulic diameter of a square heat exchanger. These improved results are attributed to an increase in mass% of ZnO in EG@DW, and surge in Reynolds. From Fig. 16a-d, it is observed that all mass% of ZnO-EG@DW nanofluids; the local Nusselt

(Nu) are grown with the rise in mass% and Reynolds (Re). While Local Nusselt numbers for all mass% decrease as the distance increases from the input point of the square shape heat exchanger. Also, at the lowest mass% of ZnO-EG@DW nanofluids, the local Nusselt (Nu) was recorded 8–13 consistent with the heat (h) at Reynolds continued from 4550 to 20,367. At the 0.05 mass% of ZnO-EG@DW-based nanofluids showing a rising trend of local Nusselt (Nu) from 6 to 15 at the similar Reynolds (Re). For 0.075 mass% of ZnO-EG@DW-based nanofluids, the local Nusselt (Nu) was perceived from 6 to 18 at the similar Reynolds (Re). Moreover, the 0.1 mass% of ZnO-EG@DW nanofluids showed a surprising enhancement in local Nusselt (Nu) about 6–25 against the specified Reynolds (Re) numbers mentioned earlier. This decreasing behavior of local Nusselt (Nu) at lowest mass% of ZnO-EG@DW-based nanofluids for all Reynolds (Re) is
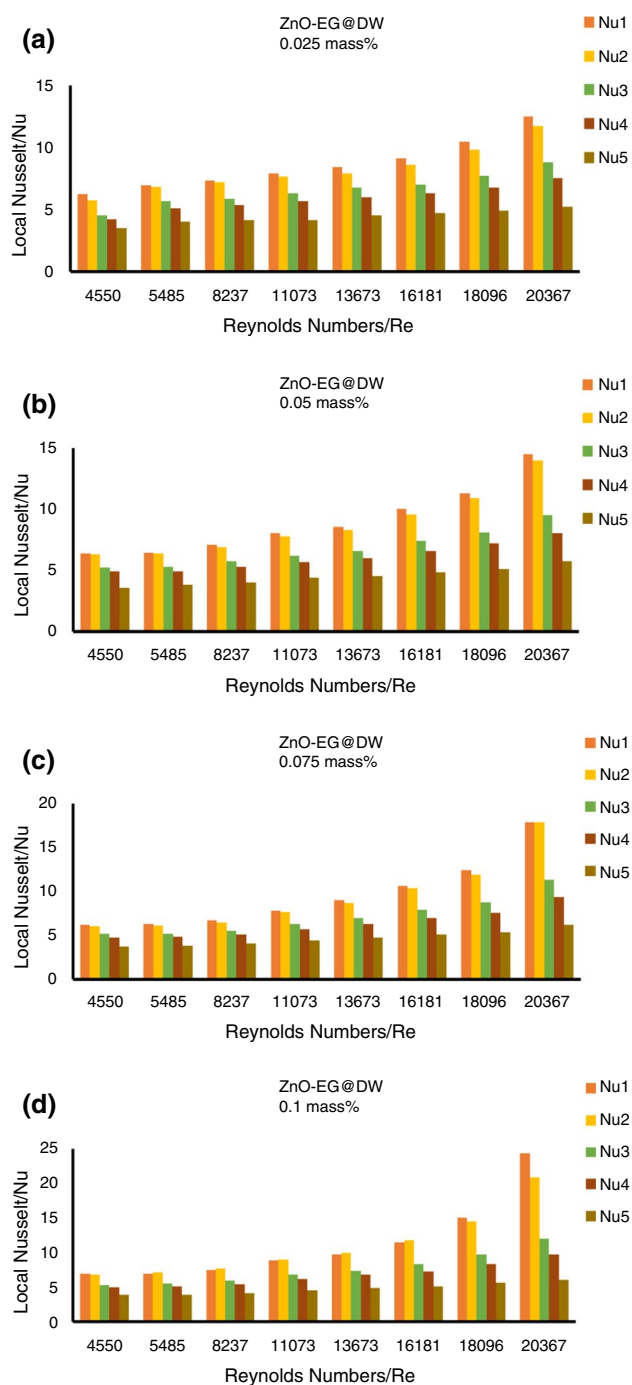
Fig. 16 a–d Local Nusselt (Nu) numbers calculation at varying mass% of ZnO-EG@DW nanofluids

attributed to the fewer amount and agglomeration of ZnO for low Reynolds. While, high Reynolds numbers stop the agglomeration of ZnO in EG@DW, which enhances the ZnO in EG@DW due to proper mixing. Finally, it has been perceived that the improvement in Nusselt numbers (Nu) is credited to a surge in heat transfer coefficient, which is ascribed to the maximum presence of ZnO nanoparticles in the base fluid.

Conclusions

The thermophysical characteristics, hydrodynamic and heat transfer (h) improvement of the ZnO-EG@DW-based nanofluids at varying mass% concentrations flowing in a square heat exchanger with constant heat flux boundaries, variable Reynolds conditions in turbulent flow regimes were studied in the current investigation. Based on experimental results the following important findings have been concluded.

- The distinctive single pot sonochemical synthesis technique for the synthesis of ZnO nanoparticles was followed by a standard high probe sonication procedure. The spherical shape of ZnO nanoparticles was produced which was confirmed by FESEM analysis.
- The ZnO-EG@DW nanofluids were prepared using a 2-step nanofluids preparation technique at four different mass% of 0.1, 0.075, 0.05, and 0.025, All the characterization tests of ZnO nanoparticles were carried out using UV–visible spectrum XRD, FTIR, and FESEM to confirm a precise synthesis.
- The experimentation was targeted to measure the thermophysical and heat transfer properties of ZnO-EG@DW-based nanofluids at varying 0.1, 0.075, 0.05, and 0.025 mass% concentrations against Reynolds (Re) numbers varied from 4550 to 20,367.
- All the mass% concentrations of ZnO-EG@DW-based nanofluids were tested for thermal conductivity measurement by using an advanced thermal analyzer (KD-2 pro). An improvement in thermal conductivity was noticed when the mass% of ZnO increases in EG@DW. The substantial augmentation in thermal conductivity was noted at 0.1 mass% concentration of the nanofluids which is greater than to the base fluid, while all other mass% shows thermal conductivity higher than base fluid and less than 0.1 mass%.
- Based on constant heat flux and variable Reynold (Re) numbers the significant improvement of heat transfer (h) was perceived at all mass% concentrations of the ZnO-EG@DW-based stable nanofluids. The highest development in heat transfer coefficient (h) was observed at 0.1 mass% concentration that is about 550–2830 W m^{-2} K^{-1} that is 63% and higher than the base fluid while, 0.25 mass% of the Nano-fluids demonstrated less improvement as compared to others.
- The ZnO-EG@DW-based nanofluids showed enhanced Nusselt (Nu) from 6 to 27 at the 0.1 mass% concentration

at the maximum value of Reynold (Re) numbers 20367. This improvement is mainly credited to the occurrence of the maximum concentration of solid ZnO nanoparticles in the base fluid.

- Thus, the improved thermal conductivity and overall heat transfer properties of ZnO-EG@DW-based nanofluids could be a good choice for heat exchangers for household and industrial applications.

Declarations

Conflict of interest The author does not have any kind of conflict.

References

1. Zubir MNM, et al. Experimental investigation on the use of reduced graphene oxide and its hybrid complexes in improving closed conduit turbulent forced convective heat transfer. Exp Therm Fluid Sci. 2015;66:290–303.
2. Bacha I, et al. Optimal model of thermal conductivity and dynamic viscosity for convective heat transfer in a nanofluid. J Nanofluid. 2019;8(1):171–8.
3. Akram N, et al. A comprehensive review on nanofluid operated solar flat plate collectors. J Therm Anal Calorim. 2020;139(2):1309–43.
4. Webb RL, Kim NJT, and Francis N, Enhanced heat transfer. 2005
5. Öğüt EB, Dilki S. Effect of prandlt number on turbulent heat transfer of corrugated trapezoidal plate heat exchangers using nanofluids. Online J Sci Technol, 201,9(2)
6. Ahmed W, et al. Effect of ZnO-water based nanofluids from sonochemical synthesis method on heat transfer in a circular flow passage. Int Commun Heat Mass Transfer. 2020;114:104591.
7. Amiri A, et al. Performance dependence of thermosyphon on the functionalization approaches: an experimental study on thermophysical properties of graphene nanoplatelet-based water nanofluids. Energy Convers Manag. 2015;92:322–30.
8. Liu ZH, et al. Thermal performance of an open thermosyphon using nanofluid for evacuated tubular high temperature air solar collector. Energy Convers Manag. 2013;73:135–43.
9. Jaisankar S, et al. Experimental studies on heat transfer and thermal performance characteristics of thermosyphon solar water heating system with helical and left–right twisted tapes. Energy Convers Manag. 2011;52(5):2048–55.
10. Tongkratoke A, et al. The experimental investigation of double pipe heat exchangers prepared from two techniques. IOP Conf Ser Mater Sci Eng. 2019;501:012064.
11. Ahmed W, et al. Characteristics investigation on heat transfer growth of sonochemically synthesized ZnO-DW based

12. nanofluids inside square heat exchanger. J Therm Anal Calorim. 2021;144(4):1517–34.
12. Choi SU, and Eastman JA, Enhancing thermal conductivity of fluids with nanoparticles, Argonne National Lab., IL (United States). 1995
13. Alawi OA, et al. Thermal conductivity and viscosity models of metallic oxides nanofluids. Int J Heat Mass Transf. 2018;116:1314–25.
14. Barai DP, et al. Reduced graphene oxide-Fe3O4 nanocomposite based nanofluids: study on ultrasonic assisted synthesis, thermal conductivity, rheology, and convective heat transfer. Ind Eng Chemistry Research. 2019;58(19):8349–69.
15. Poongavanam GK, Ramalingam V. Characteristics investigation on thermophysical properties of synthesized activated carbon nanoparticles dispersed in solar glycol. Int J Therm Sci. 2019;136:15–32.
16. Akram N, et al. Experimental investigations of the performance of a flat-plate solar collector using carbon and metal oxides based nanofluids. Energy. 2021;227:120452.
17. Chaurasia P, et al. Heat transfer augmentation in automobile radiator using Al2O3–water based nanofluid. SN Appl Sci. 2019;1(3):7.
18. Subramanya S et al. Experimental investigation of heat transfer enhancement using Water-EG-CuO based nanofluid in automotive radiator. 2019
19. Ahmed W, et al. Ultrasonic assisted new Al2O3@TiO2-ZnO/DW ternary composites nanofluids for enhanced energy transportation in a closed horizontal circular flow passage. Int Commun Heat Mass Transfer. 2021;120:105018.
20. Ahmed W, et al. Heat transfer growth of sonochemically synthesized novel mixed metal oxide ZnO+Al2O3+TiO2/DW based ternary hybrid nanofluids in a square flow conduit. Renew Sustain Energy Rev. 2021;145:111025.
21. Hosseini SSM, Dehaj MS. An experimental study on energetic performance evaluation of a parabolic trough solar collector operating with Al2O3/water and GO/water nanofluids. Energy. 2021;234:121317.
22. Said Z, et al. Enhancing the performance of automotive radiators using nanofluids. Renew Sustain Energy Rev. 2019;112:183–94.
23. Saedodin S, Zaboli M, Rostamian SH. Effect of twisted turbulator and various metal oxide nanofluids on the thermal performance of a straight tube: Numerical study based on experimental data. Chem Eng Process Process Intensif. 2020;158:108106.
24. Mahani RB, et al. Investigating the effects of different innovative turbulators on the turbulent flow field and heat transfer of a multi-phase hybrid nanofluid. J Therm Anal Calorim. 2021;143(2):1755–72.
25. Nafchi PM, et al. The evaluation on a new non-Newtonian hybrid mixture composed of TiO2/ZnO/EG to present a statistical approach of power law for its rheological and thermal properties. Phys A Stat Mech Appl. 2019;516:1–18.
26. Ahmed W, et al. One-pot sonochemical synthesis route for the synthesis of ZnO@TiO2/DW hybrid/composite nanofluid for enhancement of heat transfer in a square heat exchanger. J Therm Anal Calorim. 2020;143(2):1139–55.
27. Moldoveanu GM, et al. Al2O3/TiO2 hybrid nanofluids thermal conductivity. J Therm Anal Calorim. 2019;137(2):583–92.
28. Ahmed W, et al. Experimental investigation of convective heat transfer growth on ZnO@TiO2/DW binary composites/hybrid nanofluids in a circular heat exchanger. J Therm Anal Calorim. 2020;143(2):879–98.
29. Chen, C., et al. ZnO shape on the thermal conductivity and viscosity of ethylene glycol based nanofluids. in international heat transfer conference digital library. 2018
30. Esfe MH, et al. Modeling and prediction of rheological behavior of Al2O3-MWCNT/5W50 hybrid nano-lubricant by artificial

neural network using experimental data. Phys A Stat Mech Appl. 2018;510:625–34.

31. Toghraie DS, et al. Numerical investigation of turbulent nanofluid flow and two-dimensional forced-convection heat transfer in a sinusoidal converging-diverging channel. Heat Transf Res. 2019;50(7):671–95.

32. Ahmed W, et al. Evaluation on enhanced heat transfer using sonochemically synthesized stable Zno-Eg@Dw Nanofluids in horizontal calibrated circular flow passage. Energies. 2021;14(9):2400.

33. Fernandez-Seara J, et al. A general review of the Wilson plot method and its modifications to determine convection coefficients in heat exchange devices. Appl Therml Eng. 2007;27(17–18):2745–57.

34. Ahmed W, et al. Experimental investigation of convective heat transfer growth on ZnO@TiO2/DW binary composites/hybrid nanofluids in a circular heat exchanger. J Therm Anal Calorim. 2021;143(2):879–98.

35. Kiradjiev KB, et al. Maxwell-type models for the effective thermal conductivity of a porous material with radiative transfer in the voids. Int J Therm Sci. 2019;145:106009.

36. Ma B, et al. Estimation of measurement uncertainties for thermal conductivity of nanofluids using transient plane source (TPS) technique. In: 2018 17th IEEE intersociety conference on thermal and thermomechanical phenomena in electronic systems (ITherm). 2018

37. Petukhov BS. heat transfer and friction in turbulent pipe flow with variable physical properties. In: Hartnett JP, Irvine TF, editors. Advances in heat transfer. Netherlands p: Elsevier; 1970. p. 503–64.

38. Gnielinski V. New equations for heat and mass transfer in the turbulent flow in pipes and channels. NASA STI/recon Tech Rep A. 1975;41(1):8–16.

39. Duangthongsuk W, Wongwises S. Effect of thermophysical properties models on the predicting of the convective heat transfer coefficient for low concentration nanofluid. Int Commun Heat Mass Transfer. 2008;35(10):1320–6.

40. Blasius H, Grenzschichten in Flüssigkeiten mit kleiner Reibung. 1907: Druck von BG Teubner

41. Martínez VA, et al. Thermal characterization and stability analysis of aqueous ZnO-based nanofluids numerically implemented in microchannel heat sinks. Therm Sci Eng Progr. 2021;22:100792.

42. Upadhyaya H, et al. Green synthesis, characterization and antibacterial activity of ZnO nanoparticles. Am J Plant Sci. 2018;9(6):1279–91.

43. Shim YJ, et al. Zinc oxide nanoparticles synthesized by Suaeda japonica Makino and their photocatalytic degradation of methylene blue. Optik. 2019;182:1015–20.

44. Hu X, et al. Improving the properties of starch-based antimicrobial composite films using ZnO-chitosan nanoparticles. Carbohydr Polym. 2019;210:204–9.

45. Raja A, et al. Eco-friendly preparation of zinc oxide nanoparticles using Tabernaemontana divaricata and its photocatalytic and antimicrobial activity. J Photochem Photobiol. 2018;181:53–8.

46. Chand P, Gaur A, Kumar A. Structural and optical properties of ZnO nanoparticles synthesized at different pH values. J Alloy Compd. 2012;539:174–8.

47. Fernandes D, et al. Synthesis and characterization of ZnO CuO and a mixed Zn and Cu oxide. Matter Chem Phys. 2009;115(1):110–5.

48. Umar A, et al. Large-scale synthesis of ZnO balls made of fluffy thin nanosheets by simple solution process: structural, optical and photocatalytic properties. J Coll Interfac Sci. 2011;363(2):521–8.

49. Rani S, et al. Synthesis of nanocrystalline ZnO powder via sol–gel route for dye-sensitized solar cells. Solar Energy Mater Solar Cells. 2008;92(12):1639–45.

50. Wu L, Wu Y, Lü Y. Self-assembly of small ZnO nanoparticles toward flake-like single crystals. Mater Res Bull. 2006;41(1):128–33.

51. Missana T, Adell A. On the applicability of DLVO theory to the prediction of clay colloids stability. J Coll Interf Sci. 2000;230(1):150–6.

52. Popa I, et al. Attractive and repulsive electrostatic forces between positively charged latex particles in the presence of anionic linear polyelectrolytes. J Phys Chem B. 2010;114(9):3170–7.

53. Tang E, et al. Surface modification of zinc oxide nanoparticle by PMAA and its dispersion in aqueous system. Appl Surf Sci. 2006;252(14):5227–32.

54. Asadi A, Pourfattah F. Heat transfer performance of two oil-based nanofluids containing ZnO and MgO nanoparticles; a comparative experimental investigation. Powder Technol. 2019;343:296–308.

55. Asadi A, et al. The effect of surfactant and sonication time on the stability and thermal conductivity of water-based nanofluid containing Mg (OH) 2 nanoparticles: an experimental investigation. Int J Heat Mass Transf. 2017;108:191–8.

56. Asadi A, et al. Heat transfer efficiency of Al2O3-MWCNT/thermal oil hybrid nanofluid as a cooling fluid in thermal and energy management applications: an experimental and theoretical investigation. Int J Heat Mass Transf. 2018;117:474–86.

57. Aberoumand S, Jafarimoghaddam A. Experimental study on synthesis, stability, thermal conductivity and viscosity of Cu–engine oil nanofluid. J Taiwan Inst Chem Eng. 2017;71:315–22.

58. Li Y, et al. Experimental investigation on heat transfer and pressure drop of ZnO/ethylene glycol-water nanofluids in transition flow. Appl Therm Eng. 2016;93:537–48.

59. Nguyen CT, et al. Viscosity data for Al2O3–water nanofluid—hysteresis: is heat transfer enhancement using nanofluids reliable? Int J Therm Sci. 2008;47(2):103–11.

60. Petukhov B. Heat transfer and friction in turbulent pipe flow with variable physical properties. In: Advances in heat transfer. Elsevier; 1970. p. 503–64.